splice variant) polyclonal IgG (1:200; Chemicon International) raised against amino acid residues 535–598 of mouse versican, mouse anti–phosphacan/receptor protein tyrosine phosphatase-β (RPTPβ) core protein monoclonal IgM (1:3,000; clone 122.2; Chemicon International), mouse anti–phosphorylated neurofilament-M and -H (pNF) monoclonal IgG (1:1,000; Chemicon International), rabbit anti-ubiquitin (Ub) polyclonal IgG (1:100; Dako), and biotin-conjugated mouse anti–human neuronal protein Hu C/D monoclonal IgG (1:200; Invitrogen, Carlsbad, CA). After extensive rinsing in TBS, the sections were incubated with a combination of appropriate secondary antibodies diluted at 1:500 in an antibody diluent solution (Dako) overnight (4°C). The secondary antibodies used in this study were as follows: goat anti-mouse IgG, anti-mouse IgM, and anti-rabbit IgG conjugated to Alexa Fluor 488 (highly cross-adsorbed; Invitrogen); goat anti-rabbit IgG conjugated to Alexa Fluor 568 (highly cross-adsorbed; Invitrogen); and streptavidin conjugated to Alexa Fluor 647 (Invitrogen). After extensive washing in TBS, the slides were dipped into distilled water and coverslipped with Shandon PermaFluor (Thermo Electron Corporation, Pittsburgh, PA), then kept in the dark at 4°C until analysis. As a negative control, the above-described procedures were repeated without each primary antibody. No specific labeling was identified in these controls. For double- and triple-immunofluorescence labeling, sections were sequentially processed with each primary antibody and detected with appropriate Alexa Fluor-conjugated secondary antibodies or streptavidin as described above.

SDS-PAGE and Immunoblotting

The lumbar spinal cord was quickly removed after decapitation under deep anesthesia with diethyl ether. Each spinal cord tissue was homogenized in a lysis buffer containing 10 mM Tris-HCl, pH 7.4, 100 mM NaCl, 500 mM EDTA, and a protease inhibitor cocktail (Complete; Roche Diagnostics, Mannheim, Germany) for 30 sec at 4°C. The lysate was centrifuged at 15,000 rpm for 15 min (4°C), and the supernatant was collected and assayed for protein concentration using a Bradford assay kit (Bio-Rad Laboratories, Hercules, CA). After digestion with protease-free chondroitinase ABC (0.5 U/ml; Seikagaku, Tokyo, Japan) for 3 hr at 37°C, the protein samples were diluted with an equal amount of loading buffer [125 mM Tris-HCl, 5% wt/vol sodium dodecyl sulfate (SDS), pH 6.8], then denatured at 70°C for 5 min. SDS-polyacrylamide gel electrophoresis (SDS-PAGE) was performed in 5–10% gradient gel (Bio-Rad) for neurocan or 5–20% gradient gel (Atto, Tokyo, Japan) for phosphacan, versican, α-tubulin, and β-actin. Lysate equivalent to 3.75 μg protein sample was run on the gel for 180 min for neurocan, 450 min for versican, and 300 min for phosphacan at 100 V, together with size markers (WIDE-VIEW Western size marker; Wako Pure Chemical; Chemiluminescent-BlueRanger Prestained Molecular Weight Marker Mix; Thermo Fisher Scientific, Rockford, IL). Protein samples were then transferred to polyvinylidene difluoride (PVDF) membranes (Immobilon-P; Millipore, Bedford, MA). The membranes were blocked with 6% skim milk in TBS-T (TBS with 0.05% Tween-20) for neurocan and

phosphacan or 4% skim milk in TBS-T for versican overnight at 4°C, then incubated with a primary antibody for 1 hr at RT. The primary antibodies employed for immunoblotting were as follows: mouse anti-neurocan monoclonal IgG (1:2,000; Chemicon International); rabbit anti-GAGα domain of versican V2 polyclonal IgG (1:500; Chemicon International), mouse anti–phosphacan/RPTPβ core protein monoclonal IgM, which recognizes secreted phosphacan fragments and full-length phosphacan/RPTPβ (1:1,000; Chemicon International); mouse anti-α-tubulin monoclonal IgG (1:2,000; Sigma-Aldrich, St. Louis, MO); and mouse anti-β-actin monoclonal IgG (1:2,000; Abcam, Cambridge, United Kingdom). After three washes in TBS-T, the membranes were incubated with the appropriate horseradish peroxidase (HRP)-conjugated secondary antibody for 1 hr at RT as follows: goat anti-mouse IgG + IgM (H + L; 1:1,000; Kirkegaard and Perry Laboratories, Gaithersburg, MD), and donkey anti-rabbit IgG (1:1,000; GE Healthcare U.K.). We detected the specific bindings using an ECL Plus kit (GE Healthcare) and luminescent image analyzer (LAS-3000 mini; Fuji Photo Film, Tokyo, Japan). To ascertain specific binding of the antibody for each protein, another membrane was stained in a similar way without the primary antibody. The protein expression levels of interest were normalized to those of α-tubulin or β-actin.

Image Analysis and Quantification

We analyzed six to eight transverse sections from each lumbar spinal cord by individual immunofluorescence (n = 3–4, for each experimental group). The selected sections were separated by at least 50 μm from each other. At ×200 magnification under a confocal laser scanning microscope (CLSM) system equipped with HeNe-green (543 nm), HeNe-red (633 nm), and Ar (488 nm) laser units (FV300; Olympus Optical, Tokyo, Japan), we captured images of the defined areas (1,024 × 1,024 pixels for 352 μm × 352 μm) in the ventral horn (VH) and the ventral funiculus (VF) bilaterally, with acquisition software (Fluoview version 4.3; Olympus). The VH image was routinely obtained from the ventrolateral portion of each ventral horn, which covers Rexed's lamina IX at a maximum. The VF image was routinely obtained from the ventral superficial area of white matter in close proximity to the VH. In addition, we captured equal-sized images of the dorsal horns (Rexed's laminae III and VI) and the dorsal funiculi (between the gracile and cuneate fasciculi) for comparative analysis. On double immunofluorescence, images were captured by sequential wavelength excitation and separate detection for each wavelength in order to avoid cross-talk. The collected images were pseudocolored and merged with Fluoview (Olympus). All images of each antibody were collected at identical settings for confocal aperture, laser strength, scan velocity, photomultiplier tube sensitivity, gain, and offset. The images were digitally stored on a PC (ThinkPad; IBM Japan, Tokyo, Japan) as TIFF files with 4,095 shades of gray. We evaluated the immunoreactive area (pixels) in each defined area using computerized software (ImageJ 1.35s; Wayne Rasa, NIH). The thresholds for positive were set at constant (1,590 on 0–4,095 gray scale), and the number of

pixels above the threshold was calculated to express the CSPG-immunoreactive area. To assess the histological progression of MND phenotype, we evaluated the ubiquitin-immunoreactive area in the same way. We also estimated the number of VH neurons in the lumbar spinal cord (L5). In the captured VH images, as described above, Hu C/D-immunoreactive neurons (Liu et al., 1995) with distinct nuclei and a diameter greater than 25 μm (Gadomski et al., 2006) were counted in a fixed area (470 μm × 470 μm) using ImageJ (NIH). The average number of bilateral VH images from eight sections separated at least 50 μm from each other was submitted for statistical analysis in individual animals. For quantification of immunoblotting, the average optical densities (expressed in arbitrary units) for the specific bands were measured in ImageJ (NIH). The area showing negative immunoreaction was treated as background density. The value was normalized with the average optical densities of the immunoreactive band for α-tubulin or β-actin in each lane individually.

Statistical Analysis

All the results are expressed as mean ± SD. Differences among the rat groups were examined for significance using one-way ANOVA among means of value, with the category of rats as the independent factor. Multiple pairwise comparisons between means were tested by the Tukey-Kramer post hoc test when ANOVA showed significant differences (P < 0.05). For quantification of immunoblotting, differences between the two groups were evaluated by means of Student's t-test for paired data. All statistical analysis was performed with PC software (GraphPad Prism 5; GraphPad Software, San Diego, CA), and the null hypothesis was rejected at the 0.05 level.

RESULTS

Neuropathology in Tg Rats

To evaluate the histopathological hallmarks such as neuronal loss and abnormal protein aggregates (Watanabe et al., 2001; for review see Kabashi and Durham, 2006), we performed triple immunofluorescence for Hu C/D, pNF, and Ub in lumbar spinal cord at three different stages. The number of large ventral horn neurons we examined was immunoreactive for Hu C/D (Liu et al., 1995), with the distinct nuclei and a diameter greater than 25 μm. Therefore, the estimated number was essentially interpreted as the number of motor neurons in rat spinal cord (Gadomski et al., 2006). For the sections of non-Tg rats, we observed no significant neuronal loss or significant pNF- and Ub-immunoreactive aggregates in the ventral horns (Fig. 1Aa–c,B,C). At the Pre stage, there was no significant difference in the number of large VH neurons between Tg rats and the age-matched Non-Tg littermates (Fig. 1Aa,d,B). From the ES stage, however, the number of large VH neurons in Tg rats showed a progressive and significant decrease compared with their age-matched littermates (Fig. 1Ab,c,e,f,B; P < 0.01). The progressive loss of neurons was consistent through the disease progression, as was reported previously (Nagai et al., 2001), and was significant between

Tg rats at the Pre and ES stages (Fig. 1B; P < 0.01), whereas the statistics did not show significant difference in the symptomatic phase (between the ES and LS stages; Fig. 1B). To address the neurodegeneration aside from the neuronal loss in Tg rats, we quantified the emergence of abnormal protein aggregates in the ventral horns. From the ES stages, Tg rats showed a progressive increase of Ub- and/or pNF-immunoreactive dot- or rod-shaped aggregates in the VH neuropil (Fig. 1Ae,f). At the LS stage, we found abnormally pNF-accumulated neuronal cell body (Fig. 1Ag, arrows) with more frequent Ub- and/or pNF-immunoreactive aggregates in the ventral horns of Tg rats (Fig. 1Af,inset,g, arrows). The Ub-positive aggregates were often colocalized with or surrounded by pNF-immunoreactive structures (Fig. 1Ae,f,inset,g), suggesting intraneuronal accumulation of abnormal proteins. Furthermore, statistical analysis of immunolabeling for Ub revealed a significant and progressive increase of Ub-positive structures in Tg rats compared with non-Tg rats at the ES and LS stages (Fig. 1C; P < 0.01), and also among Tg rats at the three stages (Pre, ES, and LS; Fig. 1C; P < 0.01).

Increased CSPG Immunoreactivity in Tg Rats

To examine a possible accumulation of CSPG in the spinal cord with ALS-like motor neuron degeneration, we employed a series of immunofluorescence using antibodies specific for CSPG core proteins such as neurocan, versican, and phosphacan at different stages. In the spinal cord of non-Tg rats, mild and sparse perineuronal immunoreactivity for neurocan was observed throughout the parenchyma (Fig. 2a,e). The dorsal horns of the gray matter (data not shown) and the subpial zone of the white matter (Fig. 2e) were predominantly immunoreactive for neurocan in non-Tg sections. In contrast, Tg rats showed markedly increased immunoreactivity at all the examined stages compared with age-matched non-Tg littermates (Fig. 2b–d,f–h). Notably, the up-regulation of neurocan immunoreactivity was predominant in the ventral spinal cord (VH and VF; Fig. 2b–d,f–h) in Tg rat and spread over the dorsal spinal cord (not shown) at the symptomatic (ES and LS) stages. In addition, we frequently observed distinct perineuronal immunoreactivity for neurocan in VH of Tg rats (Fig. 2b–d, arrows). Furthermore, quantification of immunolabeling revealed a significant and progressive increase of neurocan immunoreactivity in Tg rats even from Pre stage compared with non-Tg rats. Among Tg rats, there was a significant increase of neurocan immunoreactivity in both ES and LS stages compared with Pre stage (Fig. 3).

As for versican, we detected a constitutive expression at low levels in both the gray and the white matter in non-Tg spinal cord (Fig. 2i,m). In Tg rats, versican immunoreactivity was also up-regulated in the ventral spinal cord (VH and VF) even at the Pre stage (Fig. 2j–l,n–p). Quantification of immunolabeling showed a significant increase of versican immunoreactivity in the ventral spinal cord of Tg rats compared with non-Tg rats (Fig. 3).
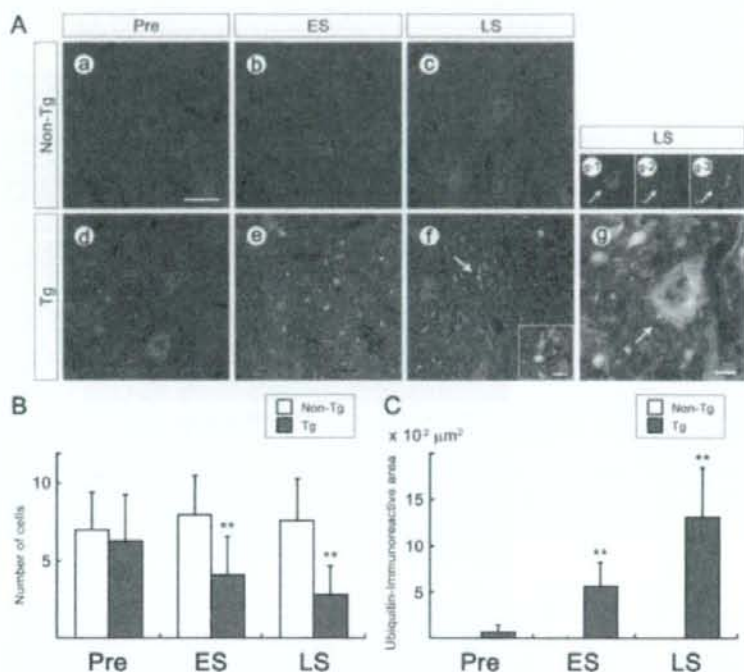
Fig. 1. Progressive pathology of spinal ventral horns in H46R trans-
genic (Tg) rats. A: Representative microphotographs of triple immu-
nofluorescence for ubiquitin (Ub, green), phosphorylated neurofila-
ment-M and -H (pNF, red), and neuronal protein Hu C/D (blue) in
ventral horns of lumbar spinal cord. Red and blue color colocaliza-
tion shows as magenta, green and blue colocalization shows as cyan,
green and red colocalization shows as yellow, and colocalization of
all three shows as white. Tg rats at presymptomatic (Pre) stage (d),
early symptomatic (ES) stage (e), and late symptomatic (LS) stage (f)
are depicted with those of age-matched littermate controls (non-Tg;
a: 24 weeks, b: 26 weeks, c: 28 weeks of age). Ub-positive deposits
were observed progressively from the ES stage (e) to the LS stage (f).
The deposits (green) were often colocalized with or surrounded by
phosphorylated neurofilament-positive structures (red) in Tg rats
[e,f(arrow and inset),g]. An abnormally pNF-accumulated neuronal
cell body was occasionally found in Tg rats (g). Hu C/D-positive
neuron (blue, g-1), pNF-positive soma (red, g-2), Ub-positive
deposits (green, g-3); g is an overlay of g-1–3). Arrows indicate a
representative large ventral horn neuron that contains Ub-positive
deposits with abnormally pNF-accumulated soma (g and g1–3).
Transverse sections are oriented so that dorsal is upward. B: A signif-
icant and progressive decrease in the number of ventral horn neurons
in Tg rats at the symptomatic stage (ES and LS). The Hu C/D-im-
munoreactive neurons (>25 µm in diameter) were counted electron-
ically with ImageJ. The progressive loss of neurons was consistent
through the disease progression, and was significant between Tg rats
at the Pre and ES stages. C: Semiquantification of the Ub immunor-
eactivity revealed a significant and progressive increase in ubiquitin-
positive deposits in the ventral horns. Open bars show the data of
age-matched non-Tg littermates, whereas solid bars show those of Tg
rats (means ± SD, n = 3 per experimental group, one-way ANOVA
followed by the Tukey-Kramer post hoc test). Asterisks indicate a
significant difference between Tg and the age-matched non-Tg rats
at each stage (**P < 0.01). Scale bars = 50 µm in f (applies to a–f);
10 µm in inset; 10 µm in g.

In contrast to neurocan, the up-regulation of versican peaked at the ES stage and diminished at the LS stage in VH of Tg rats. Among Tg rats, versican immunoreactivity in the VH was significantly higher at the ES stage compared with the Pre stage (Fig. 3). However, the versican as well as neurocan immunoreactivity in the VF showed a progressive increase in Tg rats (Fig. 3). Among Tg rats, the immunoreactivity in the VF was significantly higher at the ES and LS stage compared with the Pre stage (Fig. 3). In the dorsal horn of Tg rats as well as in the VH, the immunoreactivity for versican was significantly increased but less prominent than that in the ven-

tral horns at the ES and LS stage (data not shown). On the other hand, there was no significant difference in versican immunolabeling of the dorsal funiculi among Tg rats at the three stages (data not shown).

For phosphacan immunofluorescence, we detected low levels of immunoreactivity in non-Tg spinal cord (Fig. 4i,m). As well as neurocan, phosphacan immunor-eactivity in non-Tg was predominant in perineuronal structures in the gray matter and subpial/outer zone of the white matter (Fig. 4i,m). In contrast, Tg rats showed up-regulation of phosphacan at the symptomatic (ES and LS) stages (Fig. 4j,n). Quantification of phosphacan
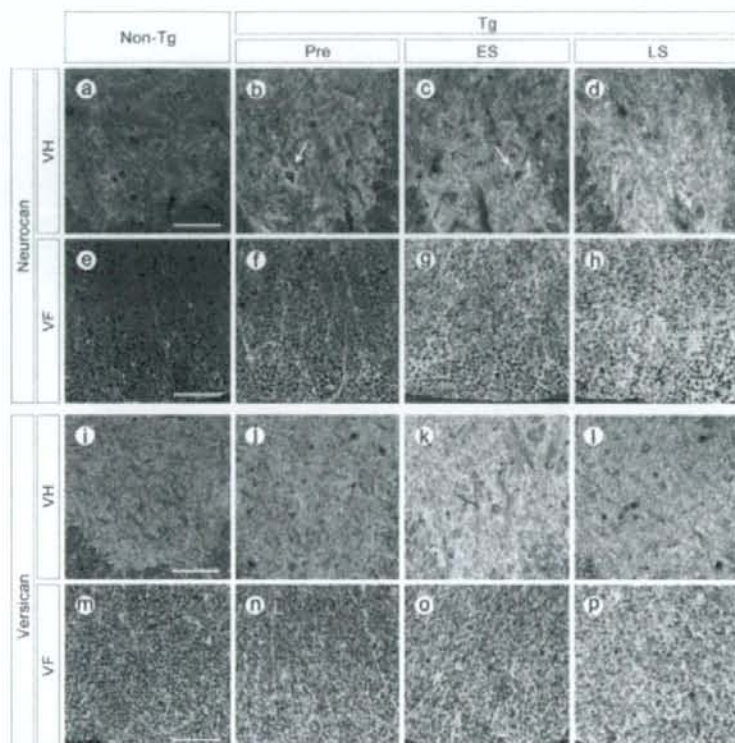
Fig. 2. Representative microphotographs of immunofluorescence for neurocan (a–h, upper panels) and versican (i–p, lower panels) in the ventral spinal cord. In H46R transgenic (Tg) rats, progressive increase of neurocan and versican immunoreactivity was observed in the ventral horns (VH: b–d,j–l) and in the ventral funiculi (VF: f–h,n–p), whereas such an increase was not observed in non-Tg rats (VH: a,i; VF: e,m). Pre, presymptomatic stage (b,f,j,n); ES, early symptomatic stage (c,g,k,o); LS, late symptomatic stage (d,h,l,p); and non-Tg: age-matched littermates corresponding to the ES stage (a,e,i,m). Arrows indicate dense neurocan immunoreactivities around neurons (b–d). Transverse sections are oriented so that dorsal is upward. Scale bars = 100 μm.

immunolabeling in VF revealed a progressive and significant increase in Tg rats at both the ES and the LS stages compared with non-Tg rats (Fig. 3). Among Tg rats, there was a significant increase of phosphacan immunoreactivity in both ES and LS stages compared with Pre stage (Fig. 3). In VH, however, we found a significant increase in Tg rats only at the ES stage (Fig. 3). At the LS stage, phosphacan immunoreactivity in VH of Tg rats returned to the normal level and was not significantly different compared with non-Tg (Fig. 3). There was no significant difference in phosphacan immunoreactivity in the dorsal horns and dorsal funiculi between Tg and Non-Tg rats at any stage (data not shown).

Association Between CSPGs and GFAP-Positive Astrocytes in Tg Rats

GFAP-positive reactive astrocytes increased even at the Pre stage, preceding loss of VH neurons in Tg rats (data not shown). As the disease progressed, the GFAP immunoreactivity became prominent continually not only in the VH but also in the white matter surrounding the VH, especially in the ventral side of spinal cord in Tg rats (Fig. 4c,g,k,o). In a similar way, Iba-1-positive

microglia increased progressively in the spinal cord of Tg rats from the Pre stage (data not shown). At the LS stage, we observed numerous hypertrophic reactive astrocytes and reactive microglia predominantly in the ventral spinal cord gray and white matter.

To clarify the cellular source of accumulated CSPGs in the spinal cord, we performed double immunofluorescence for the series of CSPG core proteins with cell type–selective markers as follows: GFAP, an astrocyte marker (Pegram et al., 1985); GST-π, mature oligodendrocytes (Tansey and Cammer, 1991; Tamura et al., 2007); neurofilament-H, large-diameter myelinated neurons (Perry and Lawson, 1993); and Iba-1, resting and activated microglia (Ito et al., 1998; Ahmed et al., 2007). The combinatorial immunolabelings revealed a partial colocalization between neurocan/phosphacan and GFAP (Fig. 4c,d,g,h for neurocan/GFAP; Fig. 4k,l,o,p for phosphacan/GFAP). Colocalization was observed predominantly in the ventral spinal cord (VH and VF), especially in the perineuronal areas immunoreactive for CSPGs in VH (Fig. 4d,l). In contrast, we did not observe any distinct colocalization between CSPGs and other cellular markers such as GST-π, neurofilament-H, and Iba-1 (data not shown).
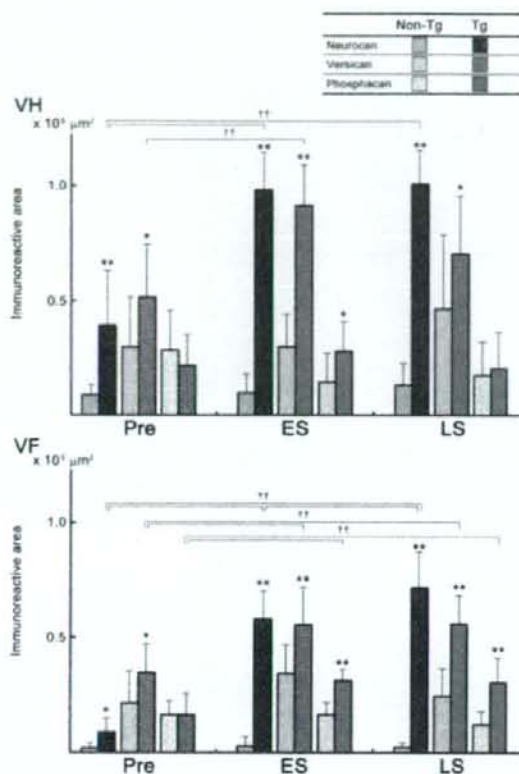
Fig. 3. Semiquantification of the immunofluorescence for different chondroitin sulfate proteoglycan core proteins in the ventral spinal cords of H46R transgenic (Tg) rats and age-matched littermate controls (non-Tg). The immunoreactive areas for various CSPG core proteins are shown by color legends in the figure. The immunoreactive areas of neurocan, versican, and phosphacan were increased in the ventral horns (VH; upper graph) and ventral funiculi (VF; lower graph) in Tg rats but not in Non-Tg rats in each stage (means ± SD, n = 3–4, one-way ANOVA followed by the Tukey-Kramer post hoc test). Asterisks indicate a significant difference between Tg and the age-matched non-Tg rats at each stage (*$P < 0.05$, **$P < 0.01$). Daggers indicate a significant difference in Tg rats between the stages (††$P < 0.01$).

Increased Levels of CSPGs in Tg Rats

To confirm the results of immunohistochemical analysis, we examined the cumulative species of CSPGs in Tg rats by quantitative immunoblotting with specific antibodies for the core proteins. According to the immunofluorescence data (Fig. 3), we selected the examined stages for the CSPG immunoblotting: LS stage for neurocan and ES stage for both versican and phosphacan. The immunoblotting revealed increased levels of distinct CSPG species in whole lumbar spinal cord lysate of Tg rats. For neurocan, immunoblotting showed increased levels of two isoforms of neurocan in the spinal

cord of Tg rats at the LS stage. In non-Tg rats, only thin bands for the proteolytic fragments of neurocan were detected at approximately 150 kDa, without specific bands for the full-length neurocan (Fig. 5A). In contrast, we detected distinct bands specific for both the full length at 245 kDa and for the proteolytic fragments at approximately 150 kDa in Tg rats (Fig. 5A). Densitometry revealed an approximately 40-fold increase of full-length neurocan and fourfold increase of proteolytic fragments of neurocan in the spinal cord of Tg rats compared with those of non-Tg rats (Fig. 5A). As for versican, we found the increased levels of the CNS-specific V2 isoform in the spinal cord of Tg rats at the ES stage. A distinct band corresponding to versican V2 at >220 kDa was evident in Tg rats, whereas very thin bands at the same molecular weight in non-Tg rats (Fig. 5B). Densitometry revealed an approximately fourfold increase of versican V2 in the spinal cord of Tg rats compared with those of non-Tg rats at the ES stage (Fig. 5B). We also found a similar result in the quantitative immunoblotting for phosphacan at the ES stage. The immunoblotting showed a smear-like band corresponding to phosphacan/RPTPβ core protein at >220 kDa. Other bands corresponding to splice variants of phosphacan were also detected at approximately 180 kDa (Fig. 5C). Densitometry revealed an approximately threefold increase of phosphacan/RPTPβ in the spinal cord of Tg rats compared with those of non-Tg rats at the ES stage. Although a similar tendency was observed in the splice variants of phosphacan, there was no significant difference between Tg rats and non-Tg rats at the stage (Fig. 5C). In contrast to the case for the ES stage, we found no significant increase in the levels of versican and phosphacan in Tg rats at the LS stage (data not shown).

DISCUSSION

In the present study, we found a significant accumulation of CSPGs in the adult spinal cord of a rat ALS model. The accumulation was predominant in the ventral spinal cord, where the neuropathology primarily occurred, and subsequently spread throughout the dorsal spinal cord. Moreover, in parallel with disease progression even from the Pre stage, we detected an accelerated increase in both neurocan and versican immunoreactivity. Therefore, it is suggested that the up-regulation of CSPGs is closely related to the neurodegeneration in the present model. However, up-regulation of phosphacan was less prominent as well as less significant only in the ES stage in the ventral horns. Previous studies have reported diverse results for phosphacan after various forms of CNS injury (McKeon et al., 1999; Moon et al., 2002; Tang et al., 2003) or demyelinating lesions (Sobel and Ahmed, 2001). Thus, the differential accumulation of CSPGs suggests a distinct property of each CSPG and a complicated regulation of CSPG metabolism under disease conditions (Galtrey and Fawcett, 2007).
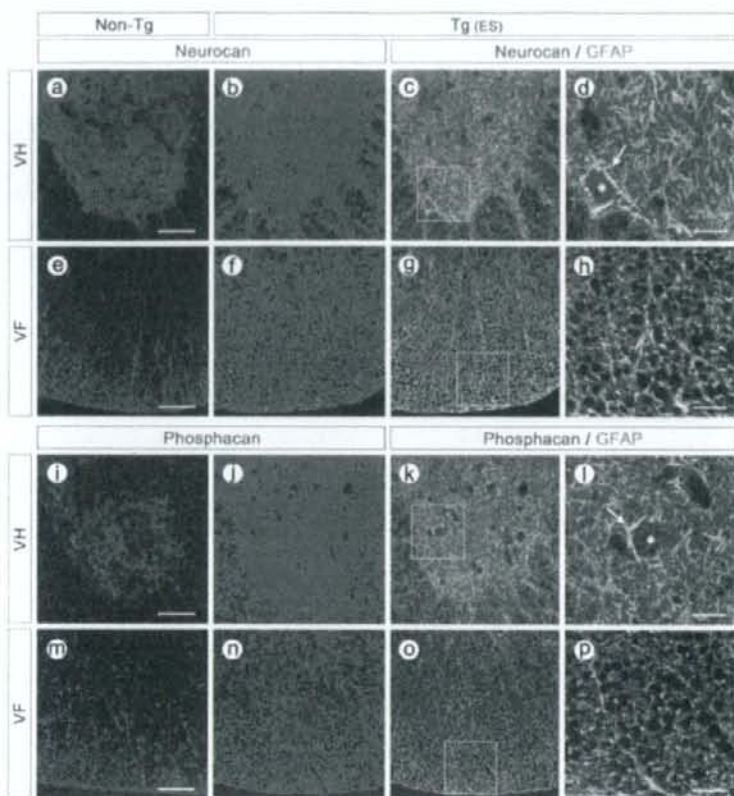
Fig. 4. Representative microphotographs of double immunofluorescence for neurocan (upper panels) or phosphacan (lower panels) with glial fibrillary acidic protein (GFAP). As shown in Figures 2 and 3, the immunofluorescence revealed up-regulation of the CSPG core proteins in the ventral horns (VH) and ventral funiculi (VF) in the spinal cord of H46R transgenic (Tg) rats at the early symptomatic (ES) stage (b,f for neurocan; j,n for phosphacan) but not in the age-matched littermate controls (non-Tg; a,e for neurocan; i,m for phosphacan). Moreover, partial colocalization of neurocan (green in c,d,g,h) or phosphacan (green in k,l,o,p) with GFAP (magenta in the same panels) was detected under confocal laser scanning microscopy in both VH and VF. Especially in VF, close colocalization was observed between neurocan/phosphacan and GFAP immunoreactivities (g,h,o,p). Images were pseudocolored and merged. Magnified view of c, g, k, and o are shown in panels d, h, l, and p, respectively. Asterisks indicate neurons that were surrounded by neurocan or phosphacan immunoreactivities; arrows indicate intense colocalization between neurocan/phosphacan and GFAP immunoreactivities around neurons (d,l). Transverse sections are oriented so that dorsal is upward. Scale bars = 100 μm in a–c,e–g,i–k,m–o; 30 μm in d,h,l,p.

CSPGs are heterogeneous, and each has its own core protein. Each core protein has a different degree of chondroitin sulfate glycosaminoglycan (GAG) chains. Neurocan, as well as versican V2 (which contains only the GAGα domain), phosphacan, and brevican, is expressed specifically in the adult CNS and constitutes a major component of the ECM. During development, CSPGs regulate axonal pathfinding, synaptogenesis, and cell migration and restrict plasticity. Furthermore, CSPGs are reported to bind and interact with a variety of molecules such as growth factors, cytokines, and cell-surface receptors. In gray matter of adult rat spinal cord,

CSPGs are distributed mainly in the neuropil, and the VH neurons are surrounded by distinct ECM containing CSPGs, which is called *perineuronal nets* (Vitellaro-Zuccarello et al., 2007). Our findings of immunofluorescence for CSPGs in non-Tg rats are fundamentally compatible with the previous report. Therefore, CSPGs play a physiologically pivotal role such as signal transmission in the intact adult spinal cord and are believed to prevent unnecessary synaptic connections for stabilizing the CNS structure.

Extensive investigations have previously revealed up-regulation of CSPGs in acute insults of CNS. In
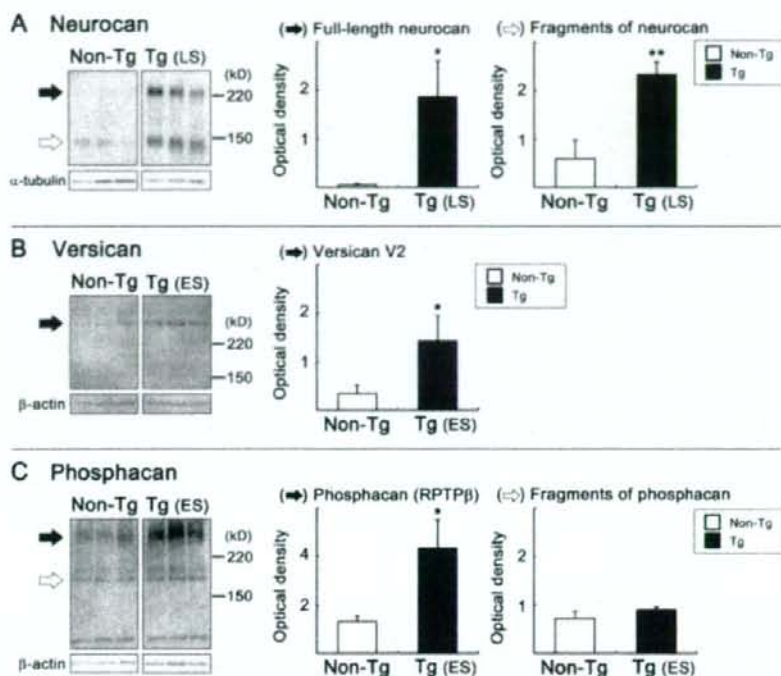
Fig. 5. Quantitative immunoblotting analysis of different chondroitin sulfate proteoglycan (CSPG) levels in the whole lumbar spinal cord of H46R transgenic (Tg) rats and the age-matched littermate controls (non-Tg). Graphs represent relative optical density value of the bands: ratios of those of CSPG to those of the internal control protein are shown (mean ± SD). Asterisks indicate a significant difference between Tg rats and non-Tg rats ($*P < 0.05$, $**P < 0.01$; n = 3, Student's t-test). A: Immunoblotting for neurocan in Tg rats at the late symptomatic (LS) stage and non-Tg controls. The level of both isoform of neurocan: the 245-kDa full-length neurocan (solid arrow) and the cleavage products (open arrow) were up-regulated (upper panel). α-Tubulin was used as an internal control for applied amounts of protein in each lane (lower panel). B: Immunoblotting for CNS-specific isoform of versican V2 in Tg rats at the early symptomatic (ES) stage and non-Tg controls. The level of versican V2 isoform (>220 kDa, solid arrow) was up-regulated (upper panel). β-Actin was used as a control (lower panel). C: Immunoblotting for phosphacan in Tg rats at the ES stage and non-Tg controls. The level of both phosphacan/RPTPβ core protein (>220 kDa, solid arrow) and the fragments (open arrow) were up-regulated (upper panel). β-Actin was used as a control (lower panel).

most cases of acute CNS insults, including cerebrocortical wound injury (McKeon et al., 1991), ischemia (Deguchi et al., 2005), demyelinating lesions (Sobel and Ahmed, 2001), kainic acid-induced excitotoxic lesions (Matsui et al., 2002; Okamoto et al., 2003), and spinal cord injury (Jones et al., 2002; Tang et al., 2003), high levels in the expression of CSPGs peak after a certain period and recover to the normal levels. We found a similar up-regulation of CSPGs even under conditions of a chronic neurodegenerative disease. However, progressive accumulation of neurocan in concert with relentless neuronal loss showed a temporal profile distinct from that of acute CNS injury. Much evidence suggests that CSPGs have inhibitory potentials on axonal regeneration in vitro and in vivo (Galtrey and Fawcett, 2007). Furthermore, more recent studies have shown that the gliosis-associated CSPGs play an additional inhibitory role in cell migration in vivo (Kearns et al., 2003;

Ikegami et al., 2005). Thus, the accumulation of CSPGs could inhibit endogenous/exogenous regenerative potential as a molecular barrier. The inhibitory property of CSPGs is derived from both the GAG side chains and the core proteins themselves. Thus, the suppression of CSPG expression or enzymatic degradation of CSPGs may change the microenvironment of spinal cord in the present model. In fact, local digestion of GAG side chains in vivo by chondroitinase ABC, a bacteria-derived enzyme, has previously been shown to induce axonal elongation and promote functional recovery in spinal cord injury models (Moon et al., 2001; Bradbury et al., 2002) and also to create a permissive environment conducive to axonal growth from peripheral nerve graft into spinal cord (Houle et al., 2006).

On the other hand, a neuroprotective role of CSPGs has also been suggested in several CNS insults, such as spinal cord injury, excitotoxicity, and β-amy-

loid-induced neurodegeneration models (Rhodes and Fawcett, 2004). Considering the possible beneficial aspects of CSPGs, the up-regulation of CSPGs surrounding residual VH neurons may reflect an endogenous protective process against the neurodegeneration in the present model. Although enzymatic digestion of CSPGs has not been reported to exacerbate CNS damage to date (Galtrey and Fawcett, 2007), the significance of the abnormally accumulated CSPGs in various types of CNS insults is still a matter of debate. Reactive gliosis, one of the prominent pathological events in ALS spinal cord (Neusch et al., 2007), consists mainly of reactive astrocytes (Silver and Miller, 2004). In addition to the astrocytic reaction, microglial activation is also an early and distinct response in Tg rodent models of ALS (Hall et al., 1998; Alexianu et al., 2001). In the present study, double immunofluorescence revealed partial associations between neurocan/phosphacan and GFAP-positive astrocytes, but not Iba-1-positive microglia, in the degenerating spinal cord of Tg rats. Hypertrophic astrocytes are principal source of neurocan and secrete it into the ECM in adult CNS. In addition, neurons are reported to synthesize neurocan. Astrocytes have also been reported to produce phosphacan following brain injury (McKeon et al., 1999; Thon et al., 2000). Consistently with these data, we observed the perineuronal dense staining around VH neurons, where GFAP-positive processes surround the neuronal cell body, in the spinal cord of Tg rats. More systematic investigation to identify the cellular source of CSPGs using this model is necessary. Because reactive astrocytes are considered to play paradoxical roles both beneficial and harmful to neurons (Sofroniew, 2005), identification of the mechanisms that regulate the molecules in the ECM could lead to control of the expression of CSPGs. In fact, a recent study demonstrated the CSPG-regulating molecules in astrocytes. Xylosyltransferase and chondroitin 4-sulfotransferase are responsible for chondroitin sulfate side chain synthesis by astrocytes (Gris et al., 2007). Transforming growth factor-β2, interleukin-6, and platelet-derived growth factor are also reported to regulate differentially the expression of CSPGs in astrocytes (Gris et al., 2007). In addition, proteases involved in the turnover of CSPG core proteins are reported, such as the matrix metalloproteinases (MMPs) and a disintegrin and metalloproteinase with thrombospondin repeats (ADAMTSs). MMPs are rapidly up-regulated after almost all types of CNS insult, including spinal cord injury (de Castro et al., 2000), ischemia (Rosenberg, 1995; Muir et al., 2002), and Alzheimer's disease (Yoshiyama et al., 2000). Further study will be needed to elucidate the possible roles of these regulatory molecules in CSPG metabolism in vivo.

Neurocan is one of the major CSPGs in the intact CNS. During development, expression of both the full-length (245 kDa) neurocan and its cleaved fragments, C-terminal (150 kDa) and N-terminal (130 kDa) neurocan, is regulated in the normal brain (Rauch et al., 1991; Meyer-Puttlitz et al., 1995). In the intact adult CNS, full-length neurocan is scarcely detected, whereas the N-

terminal fragment has been detected throughout life (Matsui et al., 1994). Moreover, both full-length and N-terminal neurocan, but not C-terminal fragments, show an inhibitory activity against neurite outgrowth (Katoh-Semba et al., 1998; Asher et al., 2000). Thus, it is suggested that full-length neurocan plays the most important role among its isoforms in regulating neural plasticity. Immunoblotting analysis in the present study showed a robust increase of the full-length neurocan and its fragments at the LS stage, further suggesting an inhibitory microenvironment for regeneration in this model. Similar changes have been reported in excitotoxic epileptic conditions (Matsui et al., 2002) and after mechanical incision, ischemia (Deguchi et al., 2005), and spinal cord injury (Tang et al., 2003). In contrast to those of neurocan, functional properties of versican, phosphacan, and their isoforms under physiological or pathological conditions remains to be established. Among three alternatively spliced variants, versican V2 is abundant in the adult CNS and is expressed by oligodendrocyte-lineage cells, whereas V1 isoform is distributed widely around the other tissue. Among the isoforms, versican V2 is considered to be inhibitory to neurite outgrowth, but how the isoforms of versican are controlled after CNS insults is unclear (Viapiano and Matthews, 2006). On the other hand, phosphacan is an extracellular part of the RPTPβ receptor, and the phosphacan/RPTPβ has at least four spliced variants. In addition to the presence of various isoforms of phosphacan/RPTPβ, their functional roles have been shown to be highly complicated. Previous reports showed diverse function (promotion or inhibition) on axonal regrowth, which depends on the mode of expression and molecules with which to interact (Faissner et al., 2006). As well as neurocan, both neurons and reactive astrocytes are reported to express phosphacan/RPTPβ. The significance of increased phosphacan in this study remains to be defined.

In summary, this is the first study to show the spatiotemporal accumulation of CSPGs under chronic neurodegenerative condition in a Tg rat model of ALS. Although the possible neuroprotective implication remains to be investigated, the increased CSPGs and their association with reactive astrocytes suggest the existence of a nonpermissive microenvironment for regeneration. Considering the future development of cell-restorative therapy in ALS, both the regulation of the microenvironment surrounding motor neurons and the control of reactive gliosis may be an important strategy in facilitating survival, migration, neurite outgrowth, and synaptogenesis of newborn cells.

ACKNOWLEDGMENTS

REFERENCES

Ahmed Z, Shaw G, Sharma VP, Yang C, McGowan E, Dickson DW. 2007. Actin-binding proteins coronin-1a and IBA-1 are effective

microglial markers for immunohistochemistry. J Histochem Cytochem 55:687–700.

Alexianu ME, Kozovska M, Appel SH. 2001. Immune reactivity in a mouse model of familial ALS correlates with disease progression. Neurology 57:1282–1289.

Aoki M, Ogasawara M, Matsubara Y, Nansawa K, Nakamura S, Itoyama Y, Abe K. 1993. Mild ALS in Japan associated with novel SOD mutation. Nat Genet 5:323–324.

Asher RA, Morgenstern DA, Fidler PS, Adcock KH, Oohira A, Braistead JE, Levine JM, Margolis RU, Rogers JH, Fawcett JW. 2000. Neurocan is upregulated in injured brain and in cytokine-treated astrocytes. J Neurosci 20:2427–2438.

Boillee S, Vande Velde C, Cleveland DW. 2006a. ALS: a disease of motor neurons and their nonneuronal neighbors. Neuron 52:39–59.

Boillee S, Yamanaka K, Lobsiger CS, Copeland NG, Jenkins NA, Kassiotis G, Kollias G, Cleveland DW. 2006b. Onset and progression in inherited ALS determined by motor neurons and microglia. Science 312:1389–1392.

Bradbury EJ, Moon LD, Popat RJ, King VR, Bennett GS, Patel PN, Fawcett JW, McMahon SB. 2002. Chondroitinase ABC promotes functional recovery after spinal cord injury. Nature 416:636–640.

Busch SA, Silver J. 2007. The role of extracellular matrix in CNS regeneration. Curr Opin Neurobiol 17:120–127.

Chi L, Ke Y, Luo C, Li B, Gozal D, Kalyanaraman B, Liu R. 2006. Motor neuron degeneration promotes neural progenitor cell proliferation, migration, and neurogenesis in the spinal cords of amyotrophic lateral sclerosis mice. Stem Cells 24:34–43.

Clement AM, Nguyen MD, Roberts EA, Garcia ML, Boillee S, Rule M, McMahon AP, Doucette W, Siwek D, Ferrante RJ, Brown RH Jr, Julien JP, Goldstein LS, Cleveland DW. 2003. Wild-type nonneuronal cells extend survival of SOD1 mutant motor neurons in ALS mice. Science 302:113–117.

de Castro RC Jr, Burns CL, McAdoo DJ, Romanic AM. 2000. Metalloproteinase increases in the injured rat spinal cord. Neuroreport 11:3551–3554.

Deguchi K, Takaishi M, Hayashi T, Oohira A, Nagotani S, Li F, Jin G, Nagano I, Shoji M, Miyazaki M, Abe K, Huh NH. 2005. Expression of neurocan after transient middle cerebral artery occlusion in adult rat brain. Brain Res 1037:194–199.

DeWitt DA, Silver J, Canning DR, Perry G. 1993. Chondroitin sulfate proteoglycans are associated with the lesions of Alzheimer's disease. Exp Neurol 121:149–152.

DeWitt DA, Richey PL, Praprotnik D, Silver J, Perry G. 1994. Chondroitin sulfate proteoglycans are a common component of neuronal inclusions and astrocytic reaction in neurodegenerative diseases. Brain Res 656:205–209.

Faissner A, Heck N, Dobbertin A, Garwood J. 2006. DSD-1-proteoglycan/phosphacan and receptor protein tyrosine phosphatase-beta isoforms during development and regeneration of neural tissues. Adv Exp Med Biol 557:25–53.

Gadomski R, Chrapusta SJ, Wojda R, Grieb P. 2006. Morphological changes and selective loss of motoneurons in the lumbar part of the spinal cord in a rat model of familial amyotrophic lateral sclerosis (fALS). Fol Neuropathol 44:154–161.

Gage FH. 2000. Mammalian neural stem cells. Science 287:1433–1438.

Galtrey CM, Fawcett JW. 2007. The role of chondroitin sulfate proteoglycans in regeneration and plasticity in the central nervous system. Brain Res Rev 54:1–18.

Gris P, Tighe A, Levin D, Sharma R, Brown A. 2007. Transcriptional regulation of scar gene expression in primary astrocytes. Glia 55:1145–1155.

Guan YJ, Wang X, Wang HY, Kawagishi K, Ryu H, Huo CF, Shimony EM, Kristal BS, Kuhn HG, Friedlander RM. 2007. Increased stem cell proliferation in the spinal cord of adult amyotrophic lateral sclerosis transgenic mice. J Neurochem 102:1125–1138.

Gurney ME, Pu H, Chiu AY, Dal Canto MC, Polchow CY, Alexander DD, Caliendo J, Hentati A, Kwon YW, Deng HX, et al. 1994. Motor neuron degeneration in mice that express a human Cu, Zn superoxide dismutase mutation. Science 264:1772–1775.

Hall ED, Oostveen JA, Gurney ME. 1998. Relationship of microglial and astrocytic activation to disease onset and progression in a transgenic model of familial ALS. Glia 23:249–256.

Haverkamp LJ, Appel V, Appel SH. 1995. Natural history of amyotrophic lateral sclerosis in a database population. Validation of a scoring system and a model for survival prediction. Brain 118:707–719.

Horner PJ, Power AE, Kempermann G, Kuhn HG, Palmer TD, Winkler J, Thal LJ, Gage FH. 2000. Proliferation and differentiation of progenitor cells throughout the intact adult rat spinal cord. J Neurosci 20:2218–2228.

Houle JD, Tom VJ, Mayes D, Wagoner G, Phillps N, Silver J. 2006. Combining an autologous peripheral nervous system "bridge" and matrix modification by chondroitinase allows robust, functional regeneration beyond a hemisection lesion of the adult rat spinal cord. J Neurosci 26:7405–7415.

Ikegami T, Nakamura M, Yamane J, Katoh H, Okada S, Iwanami A, Watanabe K, Ishii K, Kato F, Fujita H, Takahashi T, Okano HJ, Toyama Y, Okano H. 2005. Chondroitinase ABC combined with neural stem/progenitor cell transplantation enhances graft cell migration and outgrowth of growth-associated protein-43-positive fibers after rat spinal cord injury. Eur J Neurosci 22:3036–3046.

Ito D, Imai Y, Ohsawa K, Nakajima K, Fukuuchi Y, Kohsaka S. 1998. Microglia-specific localisation of a novel calcium binding protein, Iba1. Brain Res Mol Brain Res 57:1–9.

Jones LL, Yamaguchi Y, Stallcup WB, Tuszynski MH. 2002. NG2 is a major chondroitin sulfate proteoglycan produced after spinal cord injury and is expressed by macrophages and oligodendrocyte progenitors. J Neurosci 22:2792–2803.

Kabashi E, Durham HD. 2006. Failure of protein quality control in amyotrophic lateral sclerosis. Biochim Biophys Acta 1762:1038–1050.

Katoh-Semba R, Matsuda M, Watanabe E, Maeda N, Oohira A. 1998. Two types of brain chondroitin sulfate proteoglycan: their distribution and possible functions in the rat embryo. Neurosci Res 31:273–282.

Kearns SM, Laywell ED, Kukekov VK, Steindler DA. 2003. Extracellular matrix effects on neurosphere cell motility. Exp Neurol 182:240–244.

Liu J, Dalmau J, Szabo A, Rosenfeld M, Huber J, Furneaux H. 1995. Paraneoplastic encephalomyelitis antigens bind to the AU-rich elements of mRNA. Neurology 45:544–550.

Liu Z, Martin LJ. 2006. The adult neural stem and progenitor cell niche is altered in amyotrophic lateral sclerosis mouse brain. J Comp Neurol 497:468–488.

Matsui F, Watanabe E, Oohira A. 1994. Immunological identification of two proteoglycan fragments derived from neurocan, a brain-specific chondroitin sulfate proteoglycan. Neurochem Int 25:425–431.

Matsui F, Kawashima S, Shuo T, Yamauchi S, Tokita Y, Aono S, Keino H, Oohira A. 2002. Transient expression of juvenile-type neurocan by reactive astrocytes in adult rat brains injured by kainate-induced seizures as well as surgical incision. Neuroscience 112:773–781.

Matsumoto A, Okada Y, Nakamichi M, Nakamura M, Toyama Y, Sobue G, Nagai M, Aoki M, Itoyama Y, Okano H. 2006. Disease progression of human SOD1 (G93A) transgenic ALS model rats. J Neurosci Res 83:119–133.

McKeon RJ, Schreiber RC, Rudge JS, Silver J. 1991. Reduction of neurite outgrowth in a model of glial scarring following CNS injury is correlated with the expression of inhibitory molecules on reactive astrocytes. J Neurosci 11:3398–3411.

McKeon RJ, Jurynec MJ, Buck CR. 1999. The chondroitin sulfate proteoglycans neurocan and phosphacan are expressed by reactive astrocytes in the chronic CNS glial scar. J Neurosci 19:10778–10788.

Meyer-Puttlitz B, Milev P, Junker E, Zimmer I, Margolis RU, Margolis RK. 1995. Chondroitin sulfate and chondroitin/keratan sulfate proteoglycans of nervous tissue: developmental changes of neurocan and phosphacan. J Neurochem 65:2327–2337.

Moon LD, Asher RA, Rhodes KE, Fawcett JW. 2001. Regeneration of CNS axons back to their target following treatment of adult rat brain with chondroitinase ABC. Nat Neurosci 4:465–466.

Moon LD, Asher RA, Rhodes KE, Fawcett JW. 2002. Relationship between sprouting axons, proteoglycans and glial cells following unilateral nigrostriatal axotomy in the adult rat. Neuroscience 109:101–117.

Muir EM, Adcock KH, Morgenstern DA, Clayton R, von Stillfried N, Rhodes K, Ellis C, Fawcett JW, Rogers JH. 2002. Matrix metalloproteases and their inhibitors are produced by overlapping populations of activated astrocytes. Brain Res Mol Brain Res 100:103–117.

Nagai M, Aoki M, Miyoshi I, Kato M, Pasinelli P, Kasai N, Brown RH Jr, Itoyama Y. 2001. Rats expressing human cytosolic copper-zinc superoxide dismutase transgenes with amyotrophic lateral sclerosis: associated mutations develop motor neuron disease. J Neurosci 21:9246–9254.

Neusch C, Bahr M, Schneider-Gold C. 2007. Glia cells in amyotrophic lateral sclerosis: new clues to understanding an old disease? Muscle Nerve 35:712–724.

Okamoto M, Sakiyama J, Mori S, Kurazono S, Usui S, Hasegawa M, Oohira A. 2003. Kainic acid-induced convulsions cause prolonged changes in the chondroitin sulfate proteoglycans neurocan and phosphacan in the limbic structures. Exp Neurol 184:179–195.

Pegram CN, Eng LF, Wikstrand CJ, McComb RD, Lee YL, Bigner DD. 1985. Monoclonal antibodies reactive with epitopes restricted to glial fibrillary acidic proteins of several species. Neurochem Pathol 3:119–138.

Perry MJ, Lawson SN. 1993. Neurofilaments in rat and cat spinal cord; a comparative immunocytochemical study of phosphorylated and non-phosphorylated subunits. Cell Tissue Res 272:249–256.

Rauch U, Gao P, Janetzko A, Flaccus A, Hilgenberg L, Tekotte H, Margolis RK, Margolis RU. 1991. Isolation and characterization of developmentally regulated chondroitin sulfate and chondroitin/keratan sulfate proteoglycans of brain identified with monoclonal antibodies. J Biol Chem 266:14785–14801.

Reaume AG, Elliott JL, Hoffman EK, Kowall NW, Ferrante RJ, Siwek DF, Wilcox HM, Flood DG, Beal MF, Brown RH Jr, Scott RW, Snider WD. 1996. Motor neurons in Cu/Zn superoxide dismutase-deficient mice develop normally but exhibit enhanced cell death after axonal injury. Nat Genet 13:43–47.

Rhodes KE, Fawcett JW. 2004. Chondroitin sulphate proteoglycans: preventing plasticity or protecting the CNS? J Anat 204:33–48.

Rosen DR, Siddique T, Patterson D, Figlewicz DA, Sapp P, Hentati A, Donaldson D, Goto J, O'Regan JP, Deng HX, et al. 1993. Mutations in Cu/Zn superoxide dismutase gene are associated with familial amyotrophic lateral sclerosis. Nature 362:59–62.

Rosenberg GA. 1995. Matrix metalloproteinases in brain injury. J Neurotrauma 12:833–842.

Silver J, Miller JH. 2004. Regeneration beyond the glial scar. Nat Rev Neurosci 5:146–156.

Sobel RA, Ahmed AS. 2001. White matter extracellular matrix chondroitin sulfate/dermatan sulfate proteoglycans in multiple sclerosis. J Neuropathol Exp Neurol 60:1198–1207.

Sofroniew MV. 2005. Reactive astrocytes in neural repair and protection. Neuroscientist 11:400–407.

Tamura Y, Kataoka Y, Cui Y, Takamori Y, Watanabe Y, Yamada H. 2007. Intracellular translocation of glutathione S-transferase pi during oligodendrocyte differentiation in adult rat cerebral cortex in vivo. Neuroscience (in press).

Tang X, Davies JE, Davies SJ. 2003. Changes in distribution, cell association, and protein expression levels of NG2, neurocan, phosphacan, brevican, versican V2, and tenascin-C during acute to chronic maturation of spinal cord scar tissue. J Neurosci Res 71:427–444.

Tansey FA, Cammer W. 1991. A pi form of glutathione-S-transferase is a myelin- and oligodendrocyte-associated enzyme in mouse brain. J Neurochem 57:95–102.

Thon N, Haas CA, Rauch U, Merten T, Fassler R, Frotscher M, Deller T. 2000. The chondroitin sulphate proteoglycan brevican is upregulated by astrocytes after entorhinal cortex lesions in adult rats. Eur J Neurosci 12:2547–2558.

Viapiano MS, Matthews RT. 2006. From barriers to bridges: chondroitin sulfate proteoglycans in neuropathology. Trends Mol Med 12:488–496.

Vitellaro-Zuccarello L, Bosisio P, Mazzetti S, Monti C, De Biasi S. 2007. Differential expression of several molecules of the extracellular matrix in functionally and developmentally distinct regions of rat spinal cord. Cell Tissue Res 327:433–447.

Warita H, Murakami T, Manabe Y, Sato K, Hayashi T, Seki T, Abe K. 2001. Induction of polysialic acid-neural cell adhesion molecule in surviving motoneurons of transgenic amyotrophic lateral sclerosis mice. Neurosci Lett 300:75–78.

Watanabe M, Dykes-Hoberg M, Culotta VC, Price DL, Wong PC, Rothstein JD. 2001. Histological evidence of protein aggregation in mutant SOD1 transgenic mice and in amyotrophic lateral sclerosis neural tissues. Neurobiol Dis 8:933–941.

Yoshiyama Y, Asahina M, Hattori T. 2000. Selective distribution of matrix metalloproteinase-3 (MMP-3) in Alzheimer's disease brain. Acta Neuropathol 99:91–95.

A dopamine receptor antagonist L-745,870 suppresses microglia activation in spinal cord and mitigates the progression in ALS model mice

Kazunori Tanaka [a,b], Yoshinori Okada [b], Takuya Kanno [a,b,c], Asako Otomo [d], Yoshiko Yanagisawa [a,b,c], Junko Shouguchi-Miyata [a,b], Etsuko Suga [a,b], Eri Kohiki [b], Kyuichiro Onoe [b], Hitoshi Osuga [b], Masashi Aoki [e], Shinji Hadano [c,d], Yasuto Itoyama [e], Joh-E Ikeda [a,c,d,f,*]

[a] NGP Biomedical Research Institute, Neugen Pharma Inc., Tokai University School of Medicine, Isehara, Kanagawa 259-1193, Japan
[b] Department of Molecular Neuroscience, The Institute of Medical Sciences, Tokai University, Isehara, Kanagawa 259-1193, Japan
[c] Department of Molecular Life Sciences, Tokai University School of Medicine, Isehara, Kanagawa 259-1193, Japan
[d] Neurodegenerative Diseases Research Centre, Graduate School of Medicine, Tokai University, Isehara, Kanagawa 259-1193, Japan
[e] Department of Neurology, Tohoku University Graduate School of Medicine, Sendai, Miyagi 980-0872, Japan
[f] Department of Paediatrics, Faculty of Medicine, University of Ottawa, Ontario, Canada K1H 8M5

ARTICLE INFO

ABSTRACT

Amyotrophic lateral sclerosis (ALS) is a neurodegenerative disease characterized by a selective loss of motor neurons in the motor cortex, brainstem, and spinal cord. It has been shown that oxidative stress plays a pivotal role in the progression of this motor neuron loss. We have previously reported that L-745,870, a dopamine D4 receptor antagonist, selectively inhibits oxidative stress-induced cell death in vitro and exerts a potent neuroprotective effect against ischemia-induced neural cell damage in gerbil. To investigate the efficacy of L-745,870 in the treatment of ALS, we here conducted a chronic administration of L-745,870 to transgenic mice expressing a mutated form of human superoxide dismutase gene (SOD1^{H46R}); a mouse model of familial ALS, and assessed whether the mice benefit from this treatment. The pre-onset administration of L-745,870 significantly delayed the onset of motor deficits, slowed the disease progression, and extended a life span in transgenic mice. These animals showed a delayed loss of anterior horn cells in the spinal cord concomitant with a reduced level of microglial activation at a late symptomatic stage. Further, the post-onset administration of L-745,870 to the SOD1^{H46R} transgenic mice remarkably slowed the disease progression and extended their life spans. Taken together, our findings in a rodent model of ALS may have implication that L-745,870 is a possible novel therapeutic means to the treatment of ALS.

© 2008 Elsevier Inc. All rights reserved.

Introduction

Amyotrophic lateral sclerosis (ALS) is a heterogeneous group of inexorable neurodegenerative disorders characterized by a selective loss of upper motor neurons in the motor cortex, and lower motor neurons in the brainstem and spinal cord, culminating in paralysis and death. While the majority of ALS cases are sporadic, 5–10% of patients are familial ALS (fALS) (Cleveland and Rothstein, 2001), among which an approximately 20% are linked to mutations in the gene encoding copper–zinc superoxide dismutase (SOD1) (Rosen et al., 1993). Currently, there are a limited number of therapeutic strategies to effectively cure and/or relieve symptoms and improve the quality of life for patients.

Although the mechanisms for the selective degeneration of motor neurons are still unclear, several lines of evidence have indicated that ALS is associated with oxidative stress, excitotoxicity, mitochondrial

dysfunction, neurofilament accumulation, neural inflammation, and protein misfolding (Barber et al., 2006; Cluskey and Ramsden, 2001; Leichsenring et al., 2006; Menzies et al., 2002; Pasinelli and Brown, 2006; Shaw, 2005). Remarkably, the elevation of reactive oxygen species (ROS) leading to oxidative stress are shown to be associated with mitochondrial dysfunction (Barber et al., 2006; Menzies et al., 2002) and abnormal accumulation of neurofilaments in neurons (Kim et al., 2004). Further, ROS induces the disruption of glutamate uptake via glutamate transporter (EAAT2) in astrocytes, which is implicating in excitotoxic neuronal cell death (Rao et al., 2003; Rao and Weiss, 2004; Trotti et al., 1999). Thus, oxidative stress appears to play a central role in the pathogenesis for ALS.

Recently, we have identified L-745,870 as a neuronal apoptosis inhibitory protein (NAIP/BIRC1)-upregulating compound (Okada et al., 2005). NAIP is a member of the inhibitor of apoptosis protein (IAP) family and is known to exert potent protective activity against oxidative stress-induced cell death (Liston et al., 1996). In fact, although it has originally reported that L-745,870 acts as an antagonist for the dopamine D4 receptor (Patel et al., 1997), we found that L-745,870 selectively inhibited oxidative stress-induced cell death in vitro (Okada

* Corresponding author. Neurodegenerative Diseases Research Centre, Graduate School of Medicine, Tokai University Isehara, Kanagawa 259-1193, Japan. Fax: +81 463 91 4993.
E-mail address: jeikeda3@is.icc.u-tokai.ac.jp (J.-E. Ikeda).

et al., 2005). Further, it was revealed that the oral administration of L-745,870 attenuated ischemia-induced damage of the hippocampus CA1 neurons in a gerbil model (Okada et al., 2005). Taken together, L-745,870 may have a potency in the treatment of neurodegenerative diseases associated with oxidative stress, such as ALS.

Therefore, the aim of the present study was to investigate the efficacy of L-745,870 in the treatment of ALS through the study in which the systemic administration of L-745,870 to mice expressing a mutated form of human *SOD1* gene (SOD1^{H46R}) was conducted. We here demonstrated that the pre-onset administration of L-745,870 significantly retarded the disease-onset and prolonged survival in transgenic SOD1^{H46R} mice. The L-745,870 treatment also delayed loss of motor neurons in the spinal cord accompanying with the reduced level of microglial activation and TNF-α expression. Intriguingly, the post-onset administration of L-745,870 resulted in a slowed progression and prolongation of a post-onset survival span in a same mouse ALS model. Collectively, L-745,870 may provide a novel therapeutic means towards the treatment of ALS.

Materials and methods

Chemicals and antibodies

3-[[4-(4-chlorophenyl)piperazin-1-yl]methyl]-1*H*-pyrrolo[2,3-*b*] pyridine (L-745,870) (Molecular Weight: 326.82) was purchased from Ishihara Sangyo Kaisha, LTD (Siga, Japan), and subjected to animal experiments. All other chemicals are from commercial sources and of analytical grade. Antibodies used in this study included rabbit polyclonal anti-SOD1 antibody (#sc-11407; Santa Cruz), rabbit polyclonal anti-ionized calcium binding adaptor molecule 1 (Iba-1) antibody (#019-19741; Wako), rabbit polyclonal anti-glial fibrillary acidic protein (GFAP) antibody (#RB-087-A0; LAB VISION), anti-mouse TNF-α/TNFSF1A antibody (AF-410-NA; R&D SYSTEMS), and anti-nitrotyrosine antibody (#06-284, UPSTATE).

Animals

In this study, we used transgenic mice carrying the H46R mutation in the human *SOD1* gene; SOD1^{H46R} (Chang-Hong et al., 2005; Sasaki et al., 2007) as a model for fALS. Since genetic background is one of the important factors modulating disease phenotypes in mutant *SOD1* transgenic mice (Heiman-Patterson et al., 2005), we first generated congenic line of SOD1^{H46R} transgenic mice by backcrossing more than 12 generations with C57BL/6N mice, and then the line was maintained as hemizygotes by mating SOD1^{H46R} males with C57BL/6N females. The offsprings were genotyped by a PCR assay using genomic DNA from tail tissue. Mice were housed at an ambient temperature of 23 °C and at a 12 h light/dark cycle, in which water and food were available *ad libitum*. All animal experimental procedures were approved by the Tokai University Medical School Committee on Animal Care and Use.

Administration of the compound

L-745,870 was dissolved in 0.233 N HCl and then adjusted at an appropriate concentration by diluting with physiological saline. Animals were anesthetized with halothane (4%) in a mixture of N₂O/O₂ (70:30), and were intragastrically (i.g.) received with L-745,870 via a gastric tube (CAT.No.4202, Fuchigami) at a dose of either 4 mg/kg, 10 mg/kg or 20 mg/kg body weight. In parallel, two different control groups of animals; those treated with anesthesia alone (sham group) and with anesthesia followed by the vehicle administration (vehicle group), were adopted. The daily administration of L-745,870 or vehicle to mice was conducted starting at 12 weeks of age (pre-onset administration) or at the day at which animals exhibited a sign of motor dysfunction (see bellow); the onset (post-onset administration), and was continued until their terminal phase (death).

Observation of gross phenotypes in mice

Body weight of each mouse was measured from 12 weeks of age and weekly thereafter until death. Gross behavior of each animal was daily observed through visual inspection. In particular, hind limb movement and rearing behavior of each animal were weekly monitored by video camera from 12 weeks of age to the end stage. To determine the age at onset of motor dysfunction in transgenic mice, we adopted a balance beam test using the stainless steel bar (45 cm long and 0.9 cm in diameter). Motor function in the hind limbs was assessed at 12 weeks of age, and weekly thereafter until the day at which mice were unable to stay on the bar. We used the following five arbitrary grades to evaluate the motor function of mice; grade 5 (enable to walk and change the directions on the bar without their hind limb slipping), grade 4 (occasionally showed a sign of hind limb slipping, but skillfully walk on the bar), grade 3 (frequently showed a hind limb slipping, but still awkwardly walked on the bar), grade 2 (stay on the bar, but quickly fall off from the bar when attempt to walk), and grade 1 (unable to stay on the bar). In this study, the grade 3 was defined as the sign of the disease onset. Lifespan of animals was determined by the observations that mice have no longer had a heartbeat and breathing, and survival interval was calculated by the subtraction of the day of life span by the day of disease onset.

Assessment of motor function

We assessed motor performance, coordination, and balance of mice using the rotarod apparatus (MK-660A, Muromachi Kikai Co. Ltd, Japan). The duration retaining on a rod (diameter, 30 mm; rotation speed, 8 rpm; a maximum period, 120 s) without falling was measured. After the training session (20 rpm × 5 trails for 2 days), mice were tested once a week until they could no longer perform the task. Each mouse was given five trials, and the longest duration on the rod was scored.

Western blot analysis

At 13 weeks (pre-symptomatic stage; 1 week after the initial administration of L-745,870) and 22 weeks (late-symptomatic stage; after the administration of L-745,870 over a period of 10 weeks) of ages, the mice were anesthetized with halothane (4%) in a mixture of N₂O/O₂ (70:30) and transcardially perfused with physiological saline containing 10% heparin, and lumbar spinal cord was removed. Tissues were homogenized in lysis buffer (50 mM Tris–HCl (pH 7.5), 150 mM NaCl, 0.1% NP-40, Complete Protease Inhibitor Cocktail (Roche)), and was centrifuged at 22,000 ×g for 30 min. The resultant supernatant was collected as a NP-40 soluble fraction. The insoluble pellet fraction was then suspended with phosphate-buffered saline (PBS) (pH 7.2) containing 5% sodium dodecyl sulfate (SDS), sonicated, and left for 30 min at room temperature. After the centrifugation at 22,000 ×g for 30 min, the supernatant was collected as a SDS-soluble fraction. Protein concentration of each fraction was determined by the Micro BCA system (Pierce). Ten μg of protein from each fraction was electrophoretically separated on a 15% SDS-polyacrylamide gel, and transferred onto polyvinylidene difluoride (PVDF) membrane (Bio-Rad Laboratories, Hercules, CA). Membrane was blocked with 5% skimmed-milk (Wako) in TBST buffer (50 mM Tris–HCl (pH 7.4), 150 mM NaCl, 0.1% (w/v) Tween-20) overnight at 4 °C and was then incubated with the anti-SOD1 antibody (dilution 1:10,000) in TBST containing 1% skimmed-milk for 2 h at room temperature. After washing with TBST, membranes were incubated with the peroxidase-conjugated secondary anti-rabbit IgG (#NA934, GE Healthcare UK Ltd, Buckinghamshire, UK) for 1 h at room temperature. Signals were detected using ECL Plus (GE Healthcare UK Ltd).

Histopathological analysis

At 13 weeks, 19 weeks, and 22 weeks of ages, the mice were anesthetized with halothane (4%) in a mixture of N₂O/O₂ (70:30).

Under the anesthesia, the mice were transcardially perfused with physiological saline containing 10% heparin, followed by 4% paraformaldehyde (PFA) in 0.1M phosphate buffer (PB) (pH 7.2). Spinal cord was removed and post-fixed with the same fixative for 48 h at 4 °C. Lumbar segment (3–4 mm in length) was embedded in paraffin. Serial transverse sections (6 μm thickness) of lumbar segment (L4) were sliced and stained with hematoxylin and eosin (H&E) for histopathological evaluation.

Quantitative assessment of the number of anterior horn neurons in L4 lumbar segment from mice at 22 weeks of age was also conducted. Sections (6 μm thickness) were stained with cresyl-violet (Nissl staining) and observed under light microscope equipped with a CCD camera (DP71, OLYMPUS). A total of 9 representative images of every sixth serial section throughout L4 segment was analyzed. A size of neuron (cross-sectional area of each soma) was also determined by utilizing ImageJ software version 1.33u (NIH). The anterior horn neurons were counted as those fulfilled the following three criteria; 1) neurons located within ventral half of the gray matter of the spinal cord (see Fig. 4D), 2) neurons with distinct nucleolus, and 3) neurons whose the cross-sectional area was over 40 μm^2.

Immunohistochemical analysis

Immunohistochemical analyses with anti-Iba-1 (dilution 1:200), anti-GFAP (dilution 1:200), anti-TNF-α (dilution 1:50), and anti-nitrotyrosine (dilution 1:50) antibodies were performed. For immunostaining using anti-Iba-1 antibody, but not using anti-GFAP antibody, the deparaffinized sections from 22 weeks of age were pre-treated by autoclaving at 121 °C for 5 min in 10 mM citrate buffer (pH 6.0). The sections were incubated with 0.3% H_2O_2 in methanol for 30 min and then with phosphate-buffered saline (PBS) (pH 7.2) containing 0.3% Triton X-100 for 30 min. After the treatment with PBS containing 5% normal goat serum (NGS) (S-1000, Vector Laboratories) for 1 h at room temperature, the sections were incubated with either anti-Iba-1 or anti-GFAP antibody in PBS containing 1.5% NGS and 0.05% Triton X-100 overnight at 4 °C. The sections were then incubated with HISTOFINE simple stain mouse MAX-PO (R) (code 414341, Nichirei Corporation, Japan) overnight at 4 °C. The sections were visualized using 0.05% 3,3-diaminobenzidine tetrahydrochloride (DAB) (Wako) and 0.015% H_2O_2 in 50 mM Tris–HCl (pH 7.5) buffer, and the DAB reaction products were observed under a microscope.

For immunostaining using anti-TNF-α and anti-nitrotyrosine antibodies, microwave treatment of the sections from 19 weeks of age was performed for 5 min in 10 mM citrate buffer (pH 6.0). The sections were then incubated with 3% H_2O_2 for 30 min and with PBS (pH 7.2) containing 0.3% Triton X-100 for 30 min. After the treatment with PBS containing 5% normal rabbit serum (NRS) (S-5000, Vector Laboratories) or 5% NGS for 1 h at room temperature, the sections were incubated with anti-TNF-α antibody in PBS containing 1.5% NRS and 0.05% Triton X-100 or with anti-nitrotyrosine antibody in PBS containing 1.5% NGS and 0.05% Triton X-100 overnight at 4 °C. The sections were then incubated with HISTOFINE simple stain mouse MAX-PO (G) (code 414351, Nichirei Corporation, Japan) or with HISTOFINE simple stain mouse MAX-PO (R) overnight at 4 °C, and were visualized using DAB. The DAB reaction products were observed under a microscope.

Statistical analysis

Data in this study were presented as mean±SD or mean±SEM. Statistical significance was evaluated by ANOVA (analysis of variance) followed by Tukey's method for multiple comparisons between groups (Microsoft Office Excel 2003 with Excel statistics 2006). Survival data were compared using Kaplan–Meier survival analysis with log-rank test (SPSS 15.0J software). A P-value <0.05 was considered as reaching statistical significance.

Results

The L-745,870 treatment improves clinical symptoms in SOD1^{H46R} mice

In SOD1^{H46R} mice (Chang-Hong et al., 2005; Sasaki et al., 2007), the first sign of disease symptom was weakness of hind limbs, which was observed at ~17 weeks of age. As the disease progresses, abnormal gait became more apparent, and hind limb movement and rearing activity were progressively impaired. Further, when suspended by the tail, SOD1^{H46R} mice exhibited the feet-clasping like posture at an early
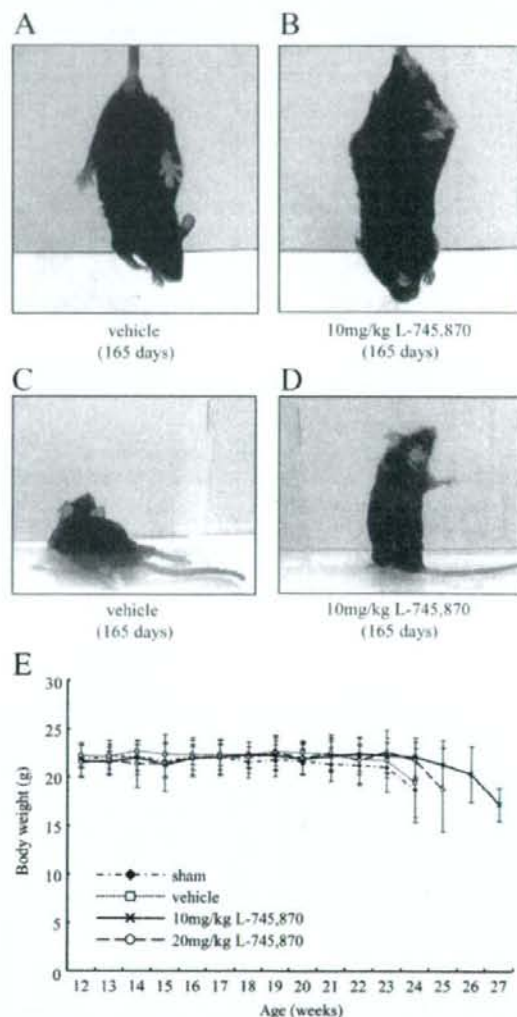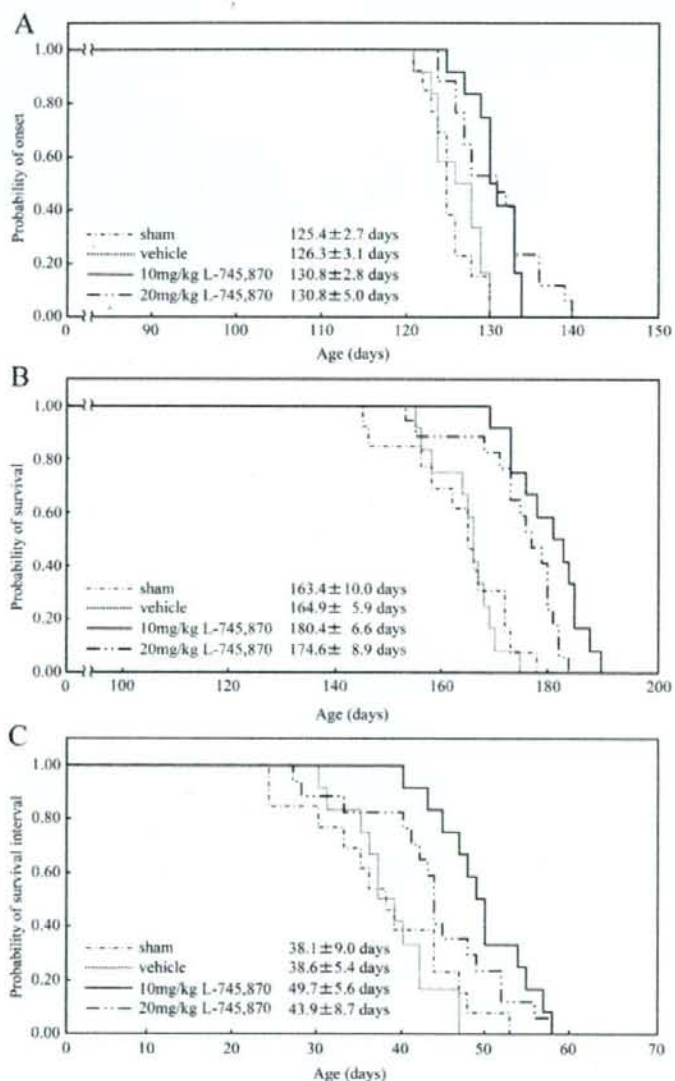

Fig. 1. Effect of the L-745,870 treatment on the gross clinical symptoms in SOD1^{H46R} mice. (A and B) Representative photographs of mice at 165 days of age showing a typical hind limb posture upon the tail suspension. The vehicle-treated mouse shows a complete paralysis in hind limb (A), whereas the L-745,870-treated mouse (10 mg/kg) still exhibits a feet-clasping phenotype (B). (C and D) Representative photographs of mice at 165 days of age showing a rearing behavior. The vehicle-treated mouse is unable to keep an upright posture (C), while those treated with L-745,870 shows a rearing behavior (D). (E) Changes in the body weight of SOD1^{H46R} mice in sham, vehicle, and L-745,870 (10 mg/kg or 20 mg/kg)-treated groups (each $n=8$). Data are expressed as mean±SD. No statistically significant differences between experimental groups were observed throughout experimental periods (12–27 weeks of age) (ANOVA). Nevertheless, it is notable that a reduction (approximately 10%) of body weight observed at the end stage of disease (23–24 weeks of age) is delayed to 25–27 weeks of age in L-745,870-treated animals.

symptomatic stage, while non-transgenic litters showed a laterally extended posture of their hind limbs (data not shown). At the end stage of disease (~23 weeks of age), they showed a complete paralysis; no movement of hind limbs, upon the tail suspension. Ultimately, the mice were unable to move and died at ~24 weeks of age.

To evaluate the effect of L-745,870 on disease symptoms, the treatment of SOD1[H46R] mice with L-745,870 was initiated at 12 weeks of age (pre-symptomatic stage). The mice were received with L-745,870 daily at a dose of either 10 mg/kg or 20 mg/kg body weight, and were monitored their hind limb movement and rearing activity. At 23 weeks

of age, a majority of the vehicle-treated mice showed a complete paralysis of hind limbs, and thus never showed a feet-clasping phenotype upon the tail suspension and a rearing behavior (Fig. 1A and C). In contrast, the L-745,870-treated mice at the same age still showed a feet-clasping phenotype and rearing activity (Fig. 1B and D).

As SOD1[H46R] mice had already reached their maximum body weight at 12 weeks of age, the effect of the L-745,870 on the weight gain could not be evaluated in this study. However, the treatment of L-745,870 prevented SOD1[H46R] mice from early weight loss (Fig. 1E) by retarding the disease progression. Incidentally, non-transgenic littermates treated

Fig. 2. Effect of the L-745,870 treatment on the disease onset and survival of SOD1[H46R] mice. The Kaplan–Meier curves demonstrate the probability of onset (A), survival (B), and survival interval (C) for sham control (n = 13), vehicle control (n = 12), 10 mg/kg L-745,870-treated (n = 12), and 20 mg/kg L-745,870-treated (n = 17) SOD1[H46R] mice. (A) The onsets were significantly delayed in 10 mg/kg and 20 mg/kg L-745,870-treated groups compared with sham control group (P < 0.001 and P = 0.001 by log-rank test, respectively), and in 10 mg/kg and 20 mg/kg L-745,870-treated groups compared with vehicle control group (P = 0.001 and P = 0.006 by log-rank test, respectively). (B) The life spans for both 10 mg/kg and 20 mg/kg L-745,870-treated groups were significant longer than those for sham and vehicle control groups (P < 0.001 by log-rank test). (C) Survival intervals after the onset were prolonged in 10 mg/kg L-745,870-treated group compared with either sham (P < 0.001 by log-rank test) or vehicle control group (P < 0.001 by log-rank test), and in 20 mg/kg L-745,870-treated group compared with vehicle control group (P = 0.013 by log-rank test). Value of the mean ± SD in each experimental group is also indicated.
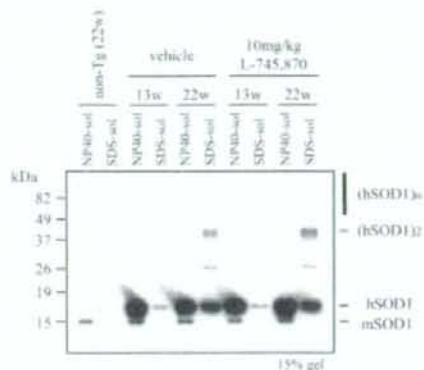
Fig. 3. Effect of the L-745,870 treatment on the mutant SOD1 level. The expression of the SOD1 protein in lumbar spinal cord from SOD1[H46R] mice (13 or 22 weeks of age) treated with vehicle or L-745,870 (10 mg/kg) and from non-transgenic (non-Tg) littermates (22 weeks of age) were examined by Western blot analysis using anti-SOD1 antibody. Tissue extracts were separated into two fractions by centrifugation; NP-40 soluble fraction (NP40-sol) and NP-40-insoluble/SDS-soluble fraction (SDS-sol). hSOD1 and mSOD1 represent the mutated (H46R) human SOD protein and endogenous mouse SOD1 protein, respectively. (hSOD1)$_2$ and (hSOD1)$_n$ indicate the dimerized and oligomerized forms of SOD1, respectively.

with L-745,870 exhibited no observable abnormalities (data not shown), indicating that the doses of the compound used in this study are not harmful to mice. Taken together, the L-745,870 treatment might improve clinical symptoms in SOD1[H46R] mice.

The administration of L-745,870 delays disease onset and progression

We next evaluated the effect of L-745,870 on the disease onset and progression in SOD1[H46R] ALS mice using the Kaplan–Meier survival analysis. The disease onset was defined at which mice showed symptom of grade 3 in balance beam test (see Materials and Methods). The mean onsets of disease for both 10 mg/kg and 20 mg/kg L-745,870-treated groups (130.8±2.8 and 130.8±5.0 postnatal days, respectively) were significantly delayed when compared with those for either sham (125.4±2.7 days) or vehicle group (126.3±3.1 days) (Fig. 2A). The life spans for both 10 mg/kg and 20 mg/kg L-745,870-treated groups (180.4±6.6 days and 174.6±8.9 days, respectively) were significantly longer than those for sham and vehicle groups (163.4±10.0 days and 164.9±5.9 days, respectively) (Fig. 2B). Further, survival intervals after the onset in L-745,870-treated animals, particularly those treated at a dose of 10 mg/kg (10 mg/kg; 49.7±5.6 days and 20 mg/kg; 43.9±8.7 days) were extended when compared with those in sham and vehicle groups (38.1±9.0 days and 38.6±5.4 days, respectively) (Fig. 2C). These results indicate that L-745,870 acts as a protective reagent against not only the onset of motor dysfunction but also the disease progression in SOD1[H46R] mice.

The L-745,870 treatment does not alter the SOD1 protein level

To ensure that the administration of L-745,870 had not altered the expression of the human SOD1 transgene in SOD1[H46R] mice, we examined the levels of the SOD1 protein in the lumbar spinal cord by Western blot analysis (Fig. 3). Endogenous mouse SOD1 (mSOD1) was
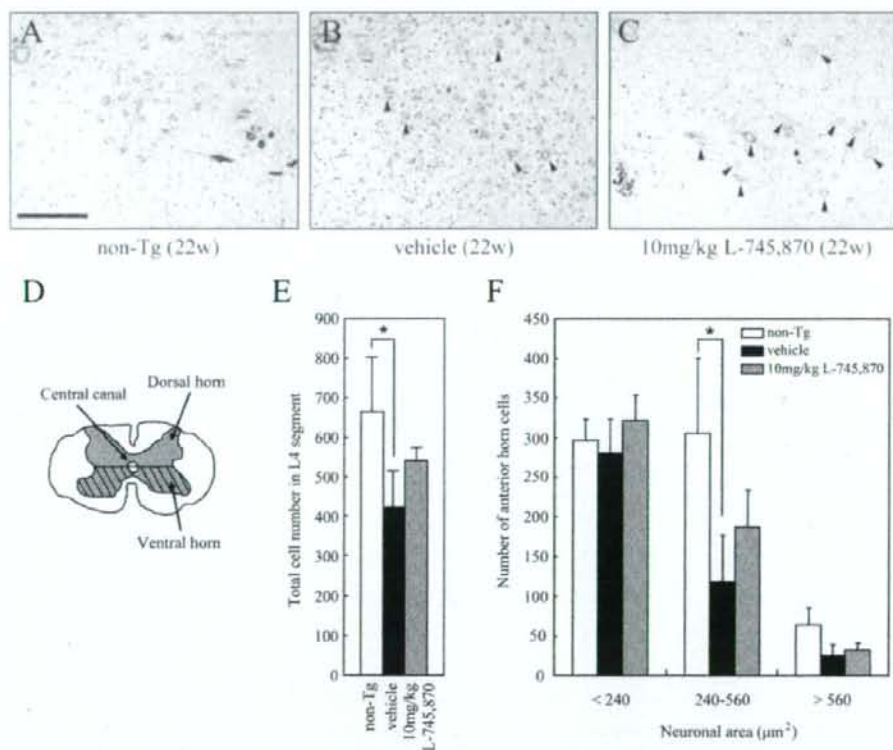
Fig. 4. Effect of the L-745,870 treatment on motor neuron loss in the spinal cord. (A–C) Representative images for the Nissl-staining of the anterior horn in the lumbar (L4) spinal cord prepared from non-transgenic (non-Tg) (A), vehicle-treated SOD1[H46R] (B), and L-745,870-treated (10 mg/kg) SOD1[H46R] (C) mice at 22 weeks of age. Arrowheads indicate spinal motor neurons. Scale bar indicates 200 μm. (D) Schematic representation of the cross-sectional L4 segment of the lumbar spinal cord. The number of the neurons within the hatched region was counted. (E) The total number and (F) the size distribution of anterior horn cells (≥40 μm²) within the ventral half of the gray matter (hatched region shown in D) in the L4 lumbar spinal cord of non-Tg (n=3), vehicle-treated SOD1[H46R] (n=3), and L-745,870 (10 mg/kg)-treated SOD1[H46R] mice (n=3) at 22 weeks of age. Data are present as mean±SD. *, P<0.05 by one-way ANOVA with Tukey's post hoc test.

present in the NP-40 soluble fractions from all animals including non-transgenic litters, while mutated human SOD1 (hSOD1) was only detected in the samples from SOD1[H46R] mice. There were no significant differences in the mutant SOD1 levels from the NP-40 soluble fractions between vehicle- and L-745,870-treated groups either at 13 weeks or 22 weeks of age. Further, although the levels of the NP-40-insoluble/SDS-soluble SOD1 protein were increased at 22 weeks of age when compared at 13 weeks of age, no significant differences in their levels between experimental groups were observed. These results indicate that L-745,870 has no apparent effect on the mutant SOD1 expression, and that the improvement of disease symptom in the L-745,870-treated animals observed in this study is not simply due to the decreased level of the mutant SOD1 protein.

The L-745,870 treatment protects from motor neuron loss

To determine whether the protective effect of L-745,870 from the progression of motor dysfunction was due to the delayed motor neuron loss, we evaluated the number of motor neurons in the spinal cord. Non-transgenic and SOD1[H46R] mice had similar motor neuron numbers at 13 week of age (pre-onset stage; data not shown). In contrast, at a late symptomatic stage (22 weeks of age), SOD1[H46R] mice treated with vehicle showed an extensive loss of large anterior horn cells (Fig. 4B) compared with non-transgenic littermate (Fig. 4A). Notably, large anterior horn cells of SOD1[H46R] mice treated with L-745,870 were relatively spared (Fig. 4C), suggesting that L-745,870 protected motor neurons from loss at a late symptomatic stage.

To confirm this notion, we conducted a quantitative analysis of the number of motor neurons whose soma sizes were larger than $40\,\mu m^2$ in the anterior horn located within ventral half of the gray matter of the spinal cord (Fig. 4D). At 22 weeks of age, SOD1[H46R] mice ($n=3$) with vehicle treatment showed a 36% loss of anterior horn cells when compared with non-transgenic littermates ($n=3$) (Fig. 4E). In contrast, L-745,870-treated SOD1[H46R] mice ($n=3$) showed a 18% loss of anterior horn cells (Fig. 4E), and a significant difference was detected in the numbers of cells between non-transgenic and vehicle-treated groups ($p<0.05$; Fig. 4E). Further, while the numbers of large anterior horn cells (240–560 μm^2) in SOD1[H46R] mice (vehicle controls) were
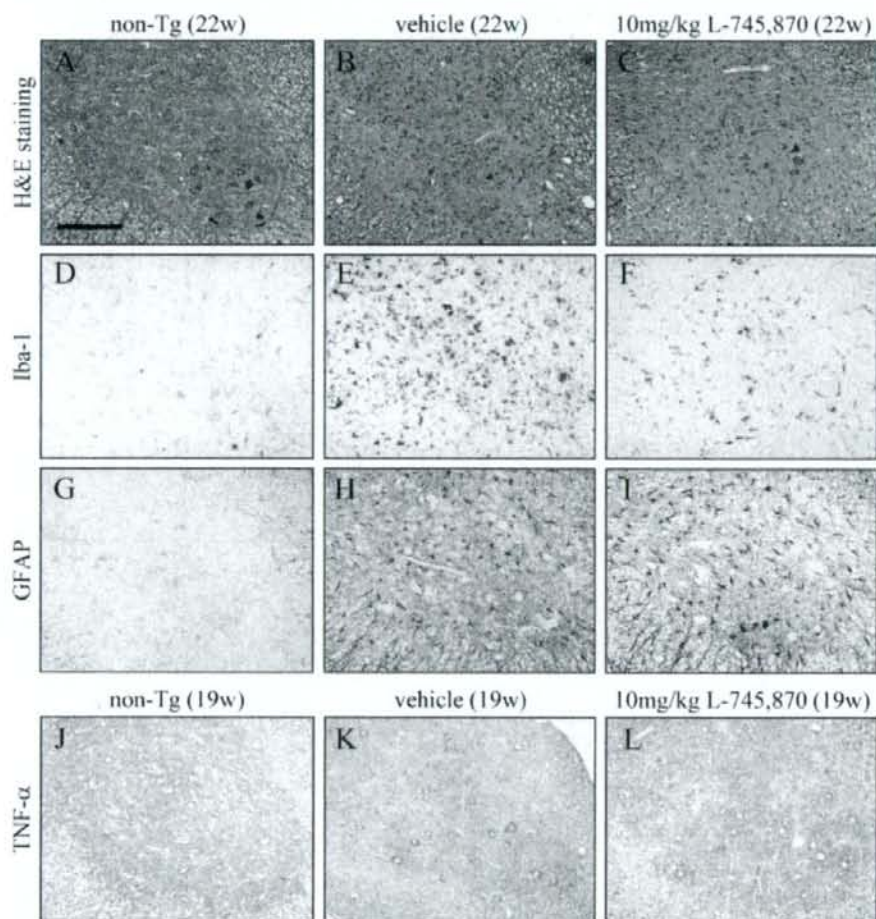

Fig. 5. Effect of the L-745,870 treatment on the activation of microglia and astrocyte and the expression of pro-inflammatory factor in the spinal cord. The lumbar spinal cord sections prepared from non-transgenic (non-Tg) (A, D, and G), vehicle-treated SOD1[H46R] (B, E, and H), and L-745,870-treated (10 mg/kg) SOD1[H46R] (C, F, and I) mice at 22 weeks of ages were stained with hematoxylin-eosin (H&E) (A–C), and immunostained with anti-Iba-1 (D–F) and anti-GFAP antibodies (G–I). The lumbar spinal cord sections prepared from non-Tg (J), vehicle-treated SOD1[H46R] (K), and L-745,870-treated (10 mg/kg) SOD1[H46R] (L) mice at 19 weeks of ages were immunostained with anti-TNF-α antibody (J–L). Scale bar indicates 200 μm.

preferentially decreased when compared with those in non-transgenic littermates (Fig. 4F), the L-745,870 treatment partly preserved such larger cells in SOD1[H46R] mice (Fig. 4F). These results indicate that L-745,870 protects motor neurons in the spinal cord from progressive degeneration in an ALS mouse model.

The L-745,870 treatment suppresses microglial activation

Microglial activation occurs from early symptomatic stage in mutant SOD1 mice (Alexianu et al., 2001; Kriz et al., 2002). To assess whether the L-745,870 treatment affects the glial cell activation at sites of motor
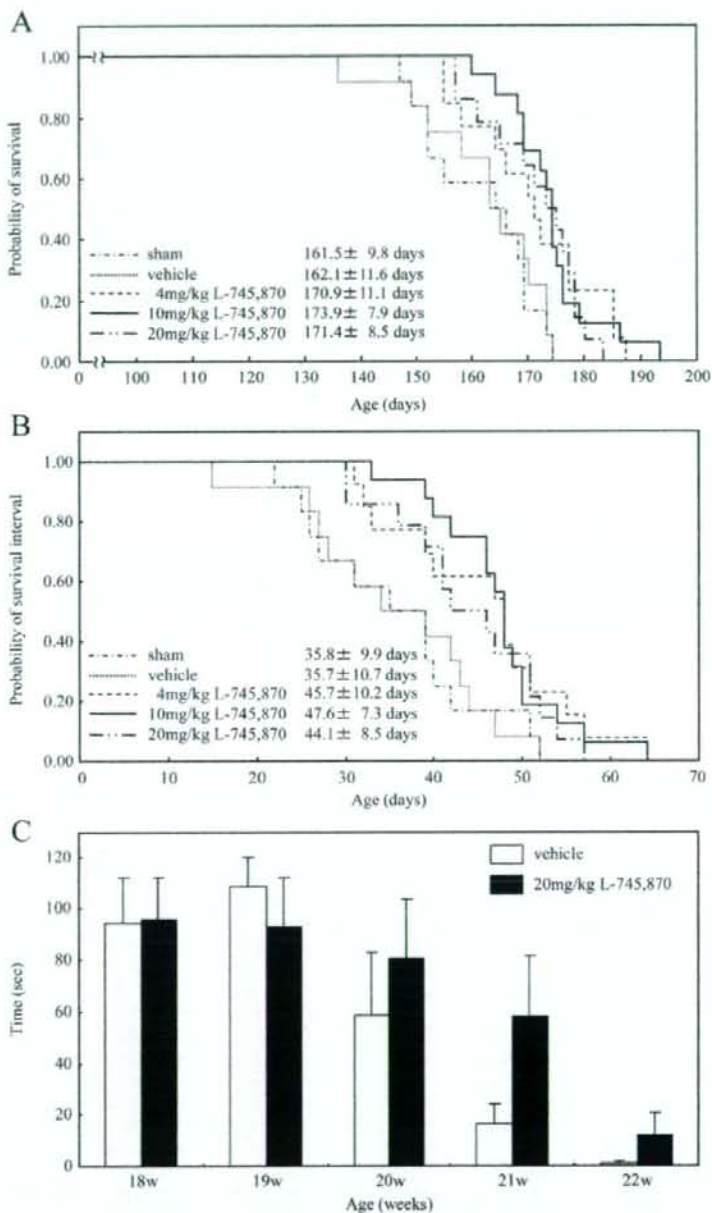
Fig. 6. Effect of the post-onset administration of L-745,870 on survival of SOD1[H46R] mice. The Kaplan–Meier curves demonstrate the probability of survival (A) and survival interval (B) of sham control (n = 12), vehicle control (n = 12), 4 mg/kg L-745,870-treated (n = 13), 10 mg/kg L-745,870-treated (n = 16), and 20 mg/kg L-745,870-treated (n = 14) SOD1[H46R] mice. The average onset of SOD1[H46R] mice was 125.9 ± 2.8 days. (A) The life spans in L-745,870-treated groups at doses of 4 mg/kg, 10 mg/kg, and 20 mg/kg were significantly extended compared with sham group (P = 0.018, P = 0.001 and P = 0.003 by log-rank test, respectively), and with vehicle group (P = 0.042, P = 0.002 and P = 0.007 by log-rank test, respectively). (B) Survival intervals in L-745,870-treated groups at doses of 4 mg/kg, 10 mg/kg, and 20 mg/kg were significantly longer than those in sham group (P = 0.038, P = 0.012 and P = 0.046 by log-rank test, respectively), and those in L-745,870-treated groups at doses of 4 mg/kg and 10 mg/kg were also longer than those in vehicle group (P = 0.019 and P = 0.003 by log-rank test, respectively). Value of the mean ± SD in each experimental group is also indicated. (C) Effect of the L-745,870 treatment on the rotarod task in SOD1[H46R] mice. The latencies to fall from the rod were scored at the ages indicated. Data are present as mean ± SEM (n = 4).

neuron loss in SOD1[H46R] ALS mice, we immunostained the lumbar sections of the spinal cord with anti-Iba-1 (marker for activated microglia) and anti-GFAP (marker for astrocytes) antibodies. At an early pre-symptomatic stage (13 weeks), there were no apparent differences in the immunoreactivity for either Iba-1 or GFAP in the lumbar spinal cord between non-transgenic, vehicle-treated SOD1[H46R], and L-745,870-treated SOD1[H46R] mice (data not shown). In contrast, at 22 weeks of age (late symptomatic stage), vehicle-treated SOD1[H46R] mice showed marked immunoreactivities both for Iba-1 and GFAP throughout the white and gray matters of the spinal cord with predominant localization in the anterior horn (Fig. 5E and H), where motor neurons were degenerated (Fig. 5B), while the lumbar spinal cord of non-transgenic siblings was almost devoid of those immunoreactivities (Fig. 5D and G). The results suggest a broad glial activation in the spinal cord of SOD1[H46R] mice at this stage. Remarkably, L-745,870-treated SOD1[H46R] mice showed a much less Iba-1 immunoreactivity in both white and gray matter of the anterior horn (Fig. 5F) and conservation of motor neurons (Fig. 5C) compared with vehicle-treated SOD1[H46R] mice (Fig. 5B and E). However, there were no observable differences in immunoreactivities for GFAP, representing a diffused astrocytic proliferation in both groups (Fig. 5H and I). Immunoblot analysis also showed the decreased levels of Iba-1 in L-745,870-treated SOD1[H46R] mice (data not shown). These results indicate that the L-745,870 treatment preferentially suppresses microglial activation, but not astrocytosis, in the spinal cord of SOD1[H46R] mice.

The L-745,870 treatment suppresses the expression of pro-inflammatory factor

To confirm whether the L-745,870 treatment suppresses the expression of pro-inflammatory factor, we carried out immunostaining of the lumbar sections from spinal cord of SOD1[H46R] ALS mice using anti-TNF-α antibody (Fig. 5J, K, and L). At 19 weeks of age, vehicle-treated SOD1[H46R] mice showed marked immunoreactivities for TNF-α (Fig. 5K) particularly in large anterior horn cells, which was consistent with the recent findings (Bigini et al., 2008; Petri et al., 2007), compared with those in non-transgenic littermates (Fig. 5J). Notably, the TNF-α immunoreactivity in the corresponding region of L-745,870-treated SOD1[H46R] mice was reduced (Fig. 5L). These results indicate that the L-745,870 treatment preferentially suppresses the expression of pro-inflammatory factor, such as TNF-α, in the spinal cord of SOD1[H46R] mice.

We further assessed whether the L-745,870 treatment suppresses the protein oxidation in the spinal cord of SOD1[H46R] ALS mice. Although the lumbar sections were broadly immunostained with anti-nitrotyrosine antibody, there were no significant differences of their immunoreactivities between vehicle-treated and L-745,870-treated SOD1[H46R] mice (data not shown).

The post-onset administration of L-745,870 prolongs survival of SOD1[H46R] mice

It is extremely crucial to evaluate whether the post-onset administration of L-745,870 improves disease symptoms. To address this issue, we conducted a daily administration of L-745,870 to SOD1[H46R] mice after showing signs of onset (125.9±2.8 days) and observed disease progression and survival. The mean life spans (± SD) of the mice treated with 4 mg/kg, 10 mg/kg and 20 mg/kg of L-745,870 were 170.9±11.1, 173.9±7.9, and 171.4±8.5 days, respectively, and significantly extended when compared with sham (161.5±9.8 days) or vehicle-treated group (162.1±11.6 days) (Fig. 6A). Further, survival intervals in L-745,870-treated animals at doses of 4 mg/kg, 10 mg/kg, and 20 mg/kg (45.7±10.2, 47.6±7.3 and 44.1±8.5 days, respectively) significantly extended longer than those in sham (35.8±9.9 days) or vehicle-treated (35.7±10.7 days) mice (Fig. 6B), and were consistent with the results of the pre-onset administration of L-745,870 (Fig. 2C). The results also showed that 10 mg/kg of L-745,870 was an optimal

dosage for exerting a potent neuroprotective efficacy in these experimental conditions. Thus, the post-onset administration of L-745,870 might effectively improve the disease symptoms and delays the disease progression in SOD1[H46R] mice.

To further assess the effect of L-745,870 on symptoms, a rotarod test was conducted using the mice treated with L-745,870 after the onset. Although no statistically significant differences between vehicle control ($n=4$) and L-745,870-treated mice ($n=4$) were observed, there was a tendency showing that the motor function of L-745,870-treated mice was preserved when compared with that of vehicle control (Fig. 6C).

Discussion

ALS is a fatal neurodegenerative disease, and there are almost no effective therapeutic strategies to cure and/or relieve symptoms and improve the quality of life for patients to date. Although the mechanisms for the selective degeneration of motor neurons are still unclear, a complex interplay between multiple pathological factors, including oxidative stress, excitotoxicity, mitochondrial dysfunction, neurofilament accumulation, neural inflammation, and protein misfolding (Barber et al., 2006; Cluskey and Ramsden, 2001; Leichsenring et al., 2006; Menzies et al., 2002; Pasinelli and Brown, 2006; Shaw, 2005), is thought to associate with pathogenesis for ALS, and thus these factors are currently proposed as therapeutic targets. Among these pathogenic factors, there is substantial evidence to support the hypothesis that oxidative stress is one of the major processes implicating in the progression of motor neuron loss (Barber et al., 2006). This study aimed to explore the novel therapeutic agent which could alleviate oxidative stress-induced neural cell damage in ALS.

The small compound L-745,870, which is a dopamine D4 receptor antagonist having an excellent oral bioavailability and brain penetration, was firstly identified as a drug candidate for antipsychotic treatment (Patel et al., 1997). However, phase IIa clinical trials of L-745,870 failed to show clinical efficacy in patients with acute schizophrenia (Bristow et al., 1997). On the other hand, we previously reported that L-745,870 selectively inhibited cell death induced by oxidative stress *in vitro* and exerted a potent neuroprotective effect *in vivo* acute ischemic model (Okada et al., 2005). In the present study, we sought to examine whether the chronic administration of L-745,870 effectively attenuates motor neuron loss in a SOD1[H46R] ALS mouse model. We here demonstrated that the pre-onset administration of L-745,870 significantly retarded the disease-onset and prolonged survival in transgenic SOD1[H46R] mice. The L-745,870 treatment also delayed loss of motor neurons in the spinal cord accompanying with the reduced level of microglial activation. Most importantly, the post-onset administration of L-745,870 resulted in a slowed progression in a same mouse ALS model.

Currently, the pharmaco-mechanisms by which L-745,870 protects motor neuron loss are still unclear. In order to investigate the mode of action of L-745,870 *in vitro*, we previously performed cell viability analyses against cell death induced by various stimuli including oxidative stressors by utilizing non-neuronal (HeLa, THP-1, and fibroblast) and neuronal (SH-SY5Y) cell cultures. As a result, the L-745,870-treatment comparatively protected all examined cell types from death induced by oxidative stressors such as menadione and H_2O_2, but not by other stimuli such as staurosporine and okadaic acid (Okada et al., 2005), suggesting that L-745,870 selectively inhibited oxidative stress-induced cell death in a cell type-independent fashion. It has been reported that the several types of dopamine receptors are expressed in SH-SY5Y cells, but not in HeLa cells (Kamakura et al., 1997; Presgraves et al., 2004). Thus, L-745,870 seems to be effective to the cells irrespective to the expression of dopamine receptors. In other words, the mode of action of this compound could be dopamine receptor-independent, although we could not completely rule out the possibility that L-745,870 exerts its potency via dopamine receptors. Alternatively, as we have originally identified L-745,870 as a NAIP-upregulating compound (Okada et al., 2005), and NAIP is known to

exert potent neuroprotective activity against oxidative stress-induced cell death (Liston et al., 1996), it is reasonable that L-745,870 exerts its potency by enhancing the NAIP-mediated cellular protection from oxidative stress in transgenic SOD1^{H46R} mice.

Several lines of evidence have demonstrated that both microglia and astrocyte were proliferated in the affected regions of ALS patients and mutant SOD1 mouse ALS models (Hall et al., 1998; Kawamata et al., 1992; Schiffer et al., 1996). Two independent groups have reported that astrocytes have an impact on motor neuron degeneration (Di Giorgio et al., 2007; Nagai et al., 2007), while others have reported that microglia contribute to non-cell-autonomous damage of neurons in neurodegenerative diseases (Block et al., 2007; Liu and Hong, 2003; Moisse and Strong, 2006). Further, it has also been proposed that chromogranin-mediated secretion of mutant SOD1 from neurons and astrocytes enhances microgliosis and motor neuron death (Urushitani et al., 2006). These studies suggest a contribution of non-neuronal cells to the ALS pathogenesis. In the present study, we showed that L-745,870 suppressed the activation of microglia, but not astrocytosis, in the spinal cord of SOD1^{H46R} mice. Further, L-745,870 suppresses the upregulation of pro-inflammatory factor (TNF-α) but not the oxidative modification of proteins (nitrated proteins) in motor neurons. Recently, it has been reported that the activation of NADPH oxidase generating ROS from microglia promotes motor neuron degeneration in the spinal cord (Wu et al., 2006). NADPH oxidase, which is a membrane-bound enzyme and catalyzes the production of superoxide from oxygen, has been implicated as an important source of microglial-derived ROS generation (Block et al., 2007). It has also been shown that the production of pro-inflammatory factors is induced by ROS (Barber et al., 2006). Thus, the L-745,870 treatment may attenuate the microglia activation and coordinately suppress the expression of TNF-α in the spinal cord, which in turn results in the protection from motor neuron loss.

In conclusions, our findings in a rodent model of ALS, demonstrating an obvious neuroprotective efficacy of L-745,870, may have implication that L-745,870 is a promising candidate as a potential therapeutic drug to the treatment of ALS. Moreover, as reactive microglia have identified in the spinal cord from sporadic ALS patients (Kawamata et al., 1992), L-745,870 might be useful not only for familial but also for sporadic ALS. Although the mode of action of L-745,870 on motor neuron protection is not fully understood, future studies on the target analysis of L-745,870 *in vivo* will clarify more therapeutic potential of L-745,870 in ALS and other neurodegenerative diseases.

Acknowledgments

References

Alexianu, M.E., Kozovska, M., Appel, S.H., 2001. Immune reactivity in a mouse model of familial ALS correlates with disease progression. Neurology 57, 1282–1289.
Barber, S.C., Mead, R.J., Shaw, P.J., 2006. Oxidative stress in ALS: a mechanism of neurodegeneration and a therapeutic target. Biochim. Biophys. Acta 1726, 1051–1067.
Bigini, P., Repici, M., Cantarella, G., Fumagalli, E., Barbera, S., Cagnotto, A., De Luigi, A., Tonelli, R., Bernardini, R., Borsello, T., Mennini, T., 2008. Recombinant human TNF-binding protein-1 (rhTBP-1) treatment delays both symptoms progression and motor neuron loss in the wobbler mouse. Neurobiol. Dis. doi:10.1016/j.nbd.2007.11.005.
Block, M.L., Zecca, L., Hong, J.-S., 2007. Microglia-mediated neurotoxicity: uncovering the molecular mechanisms. Nat. Rev. Neurosci. 8, 57–69.
Bristow, L.J., Kramer, M.S., Kulagowski, J., Patel, S., Ragan, C.I., Seabrook, G.R., 1997. Schizophrenia and L-745,870, a novel dopamine D4 receptor antagonist. Trends Pharmacol. Sci. 18, 186–188.
Chang-Hong, R., Wada, M., Koyama, S., Kimura, H., Arawaka, S., Kawanami, T., Kurita, K., Kadoya, T., Aoki, M., Itoyama, Y., Kato, T., 2005. Neuroprotective effect of oxidized galectin-1 in a transgenic mouse model of amyotrophic lateral sclerosis. Exp. Neurol. 194, 203–211.
Cleveland, D.W., Rothstein, J.D., 2001. From Charcot to Lou Gehrig: deciphering selective motor neuron death in ALS. Nat. Rev. Neurosci. 2, 806–819.
Cluskey, S., Ramsden, D.B., 2001. Mechanisms of neurodegeneration in amyotrophic lateral sclerosis. J. Clin. Pathol: Mol. Pathol. 54, 386–392.
Di Giorgio, F.P., Carrasco, M.A., Siao, M.C., Maniatis, T., Eggan, K., 2007. Non-cell autonomous effect of glia on motor neurons in an embryonic stem cell-based ALS model. Nat. Neurosci. 10, 608–614.
Hall, E.D., Oostveen, J.A., Gurney, M.E., 1998. Relationship of microglial and astrocytic activation to disease onset and progression in a transgenic model of familial ALS. Glia 23, 249–256.
Heiman-Patterson, T.D., Deitch, J.S., Blankenhorn, E.P., Erwin, K.L., Perreault, M.J., Alexander, B.K., Byers, N., Toman, I., Alexander, G.M., 2005. Background and gender effects on survival in the TgN(SOD1-G93A)1Gur mouse model of ALS. J. Neurol. Sci. 236, 1–7.
Kamakura, S., Iwaki, A., Matsumoto, M., Fukumaki, Y., 1997. Cloning and characterization of the 5'-flanking region of human dopamine D4 receptor gene. Biochem. Biophys. Res. Commun. 235, 321–326.
Kawamata, T., Akiyama, H., Yamada, T., McGeer, P.L., 1992. Immunologic reactions in amyotrophic lateral sclerosis brain and spinal cord tissue. Am. J. Pathol. 140, 691–707.
Kim, N.H., Jeong, M.S., Choi, S.Y., Kang, J.H., 2004. Oxidative modification of neurofilament-L by the Cu,Zn-superoxide dismutase and hydrogen peroxide system. Biochimie 86, 553–559.
Kriz, J., Nguyen, M.D., Julien, J.-P., 2002. Minocycline slows disease progression in a mouse model of amyotrophic lateral sclerosis. Neurobiol. Dis. 10, 268–278.
Léichsenring, A., Linnartz, B., Zhu, X.R., Lübbert, H., Stichel, C.C., 2006. Ascending neuropathology in the CNS of a mutant SOD1 mouse model of amyotrophic lateral sclerosis. Brain Res. 1096, 180–195.
Liston, P., Roy, N., Tamai, K., Lefebvre, C., Baird, S., Cherton-Horvat, G., Farahani, R., McLean, M., Ikeda, J.-E., MacKenzie, A., Korneluk, R.G., 1996. Suppression of apoptosis in mammalian cells by NAIP and a related family of IAP genes. Nature 379, 349–353.
Liu, B., Hong, J.-S., 2003. Role of microglia in inflammation-mediated neurodegenerative diseases: mechanisms and strategies for therapeutic intervention. J. Pharmacol. Exp. Ther. 304, 1–7.
Menzies, F.M., Ince, P.G., Shaw, P.J., 2002. Mitochondrial involvement in amyotrophic lateral sclerosis. Neurochem.Int. 40, 543–551.
Moisse, K., Strong, M.J., 2006. Innate immunity in amyotrophic lateral sclerosis. Biochim. Biophys. Acta 1726, 1083–1093.
Nagai, M., Re, D.B., Nagata, T., Chalazonitis, A., Jessell, T.M., Wichterle, H., Przedborski, S., 2007. Astrocytes expressing ALS-linked mutated SOD1 release factors selectively toxic to motor neurons. Nat. Neurosci. 10, 615–622.
Okada, Y., Sakai, H., Kohiki, E., Suga, E., Yanagisawa, Y., Tanaka, K., Hadano, S., Osuga, H., Ikeda, J.-E., 2005. A dopamine D4 receptor antagonist attenuates ischemia-induced neuronal cell damage via upregulation of neuronal apoptosis inhibitory protein. J. Cereb. Blood Flow Metab. 25, 794–806.
Pasinelli, P., Brown, R.H., 2006. Molecular biology of amyotrophic lateral sclerosis: insights from genetics. Nat. Rev. Neurosci. 7, 710–723.
Patel, S., Freedman, S., Chapman, K.L., Emms, F., Fletcher, A.E., Knowles, M., Marwood, R., Mcallister, G., Myers, J., Curtis, N., Kulagowski, J.J., Leeson, P.D., Ridgill, M., Graham, M., Matheson, S., Rathbone, D., Watt, A.P., Bristow, L.J., Rupniak, N.M., Baskin, E., Lynch, J.J., Ragan, C.I., 1997. Biological profile of L-745,870, a selective antagonist with high affinity for the dopamine D4 receptor. J. Pharmacol.Exp. Ther. 283, 636–647.
Petri, S., Calingasan, N.Y., Alsaied, O.A., Wille, E., Kiaei, M., Friedman, J.E., Baranova, O., Chavez, J.C., Beal, M.F., 2007. The lipophilic metal chelators DP-109 and DP-460 are neuroprotective in a transgenic mouse model of amyotrophic lateral sclerosis. J. Neurochem. 102, 991–1000.
Presgraves, S.P., Borwege, S., Millan, M.J., Joyce, J.N., 2004. Involvement of dopamine D(2)/D(3) receptors and BDNF in the neuroprotective effects of S32504 and pramipexole against 1-methyl-4-phenylpyridinium in terminally differentiated SH-SY5Y cells. Exp. Neurol. 190, 157–170.
Rao, S.D., Yin, H.Z., Weiss, J.H., 2003. Disruption of glial glutamate transport by reactive oxygen species produced in motor neurons. J. Neurosci. 23, 2627–2633.
Rao, S.D., Weiss, J.H., 2004. Excitotoxic and oxidative cross-talk between motor neurons and glia in ALS pathogenesis. Trends Neurosci. 27, 17–23.
Rosen, D.R., Siddique, T., Patterson, D., Figlewicz, D.A., Sapp, P., Hentati, A., Donaldson, D., Goto, J., O'Regan, J.P., Deng, H.-X., Rahmani, Z., Krizus, A., McKenna-Yasek, D., Cayabyab, A., Gaston, S.M., Berger, R., Tanzi, R.E., Halperin, J.J., Herzfeldt, B., Van den Bergh, R., Hung, W.-Y., Bird, T., Deng, G., Mulder, D.W., Smyth, C., Laing, N.G., Soriano, E., Pericak-Vance, M.A., Haines, J., Rouleau, G.A., Gusella, J.S., Horvitz, H., Brown Jr., R. R.H., 1993. Mutations in Cu/Zn superoxide dismutase gene are associated with familial amyotrophic lateral sclerosis. Nature 362, 59–62.
Sasaki, S., Nagai, M., Aoki, M., Komori, T., Itoyama, Y., Iwata, M., 2007. Motor neuron disease in transgenic mice with an H46R mutant SOD1 gene. J. Neuropathol. Exp. Neurol. 66, 517–524.
Schiffer, D., Cordera, S., Cavalla, P., Migheli, A., 1996. Reactive astrogliosis of the spinal cord in amyotrophic lateral sclerosis. J. Neurol. Sci. 139 (Suppl.), 27–33.
Shaw, P.J., 2005. Molecular and cellular pathways of neurodegeneration in motor neurone disease. J. Neurol. Neurosurg. Psychiatry 76, 1046–1057.
Trotti, D., Rolfs, A., Danbolt, N.C., Brown Jr., R.H., Hediger, M.A., 1999. SOD1 mutants linked to amyotrophic lateral sclerosis selectively inactivate a glial glutamate transporter. Nat. Neurosci. 2, 427–433.
Urushitani, M., Sik, A., Sakurai, T., Nukina, N., Takahashi, R., Julien, J.-P., 2006. Chromogranin-mediated secretion of mutant superoxide dismutase proteins linked to amyotrophic lateral sclerosis. Nat. Neurosci. 9, 108–118.
Wu, D.-C., Ré, D.B., Nagai, M., Ischiropoulos, H., Przedborski, S., 2006. The inflammatory NADPH oxidase enzyme modulates motor neuron degeneration in amyotrophic lateral sclerosis mice. Proc. Natl. Acad. Sci. U.S.A. 103, 12132–12137.

Up-Regulation of Insulin-Like Growth Factor-II Receptor in Reactive Astrocytes in the Spinal Cord of Amyotrophic Lateral Sclerosis Transgenic Rats

BYAMBASUREN DAGVAJANTSAN,[1] MASASHI AOKI,[1] HITOSHI WARITA,[1] NAOKI SUZUKI[1] and YASUTO ITOYAMA[1]

[1]Department of Neurology, Tohoku University Graduate School of Medicine, Sendai, Japan

Amyotrophic lateral sclerosis (ALS) is a fatal neurodegenerative disease caused by selective motor neuron death. We developed a rat model of ALS expressing a human cytosolic copper-zinc superoxide dismutase (SOD1) transgene with two ALS-associated mutations: glycine to alanine at position 93 (G93A) and histidine to arginine at position 46 (H46R). Although the mechanism of ALS is still unclear, there are many hypotheses concerning its cause, including loss of neurotrophic support to motor neurons. Recent evidence suggests that insulin-like growth factors (IGFs) act as neurotrophic factors, and promote the survival and differentiation of neuronal cells including motor neurons. Their ability to enhance the outgrowth of spinal motor neurons suggests their potential as a therapeutic agent for the patients with ALS. In this study, we investigated IGF-II receptor immunoreactivity in the anterior horns of the lumbar level of the spinal cord in SOD1 transgenic rats with the H46R mutation of different ages as well as in normal littermates. The double-immunostaining for IGF-II receptor and glial fibrillary acidic protein (GFAP) demonstrated co-localization on reactive astrocytes ($**p < 0.001$) in the end-stage transgenic rats, whereas it was not evident at the pre-symptomatic stage or at the onset of the disease. Our results demonstrated the IGF-II receptor up-regulation in reactive astrocytes in the spinal cord of transgenic rats, which may reflect a protective response against the loss of IGF-related trophic factors. We suggest that IGF receptors may play a key role in the pathogenesis, and may have therapeutic implications in ALS. ———— amyotrophic lateral sclerosis; insulin-like growth factor; transgenic rat; IGF receptor; SOD1

Amyotrophic lateral sclerosis (ALS) is a fatal neurodegenerative disease caused by selective motor neuron death. Approximately 10% of cases of ALS are inherited, usually as an autosomal dominant trait. In ~25% of familial cases, the disease is caused by mutations in the gene encoding cytosolic copper-zinc superoxide dismutase (SOD1)(Aoki et al. 1993; Rosen 1993). The overexpression of mutant human SOD1 in mice is used as model for ALS, however, some experimental manipulations are difficult in transgenic (Tg) mice because of size limitations. Thus, we developed a rat model of ALS expressing a human SOD1 transgene with two ALS-associated mutations: glycine to alanine at

303